國 立 交 通 大 學

電機學院通訊與網路科技產業研發碩士班

碩 士 論 文

適用於Bluetooth /Zigbee / Wi-Fi 頻帶之共平面帶線柴氏帶通濾波器

Coplanar Stripline Bandpass Filter with Tchebyshev Response for Bluetooth / Zigbee / Wi-Fi Applications

研 究 生：施逸銘
指 導 教 授：張志揚 博士

中華民國 九十七 年 六 月

適用於Bluetooth /Zigbee / Wi-Fi 頻帶之共平面帶線柴氏帶通濾波器

Coplanar Stripline Bandpass Filter with Tchebyshev Response for Bluetooth / Zigbee / Wi-Fi Applications

研　究　生：施逸銘　　Student : Yi-Ming Shih

指　導　教　授：張志揚 博士　　Advisor : Dr. Chi-Yang Chang

國 立 交 通 大 學

電機學院通訊與網路科技產業研發碩士班

碩士論文

A Thesis

Submitted to College of Electrical and Computer Engineering

National Chiao Tung University

in partial Fulfillment of the Requirements

for the Degree of

in

Industrial Technology R and D Master Program on

Communication Engineering

June 2008

HsinChu, Taiwan, Republic of China

中華民國九十七年六月

適用於Bluetooth /Zigbee / Wi-Fi 頻帶之共平面帶線柴氏帶通濾波器

研究生: 施逸銘　　　　　　　　　　指 導 教 授: 張志揚 博士

國立交通大學電機學院產業研發碩士班

摘　　要

本論文研製之共平面帶線柴氏帶通濾波器是利用導納轉換器與阻抗轉換器建立其等效模型; 並搭配四分之一與二分之一波長諧振器來設計具有柴氏響應之帶通濾波器. 使用共平面帶線實現電路具有差動式輸出入, 無需貫孔接地與空橋, 且不受基板後厚度影響並可達到高特性阻抗, 非常適合於平衡式無線通訊系統與射頻積體電路.

Coplanar Stripline Bandpass Filter with Tchebyshev Response for Bluetooth / Zigbee / Wi-Fi Applications

Student: Yi-Ming Shih Advisor: Dr. Chi-Yang Chang

Industrial Technology R and D Master Program of
Electrical and Computer Engineering College
National Chiao Tung University

Abstract

Filter design procedure is using the equivalent J and K inverter model in cooperation with $\lambda/2$ and $\lambda/4$ resonators to achieve Tchebyshev response, and using the CPS to implement circuit with differential I/O. The proposed circuit has the benefits of no need via holes or air-bridges, insensitive to the variation of substrate thickness, and relatively higher characteristic impedances. The proposed filters are very suitable for differential wireless communication system and radio-frequency integrated circuits.

Acknowledgement

誌謝

首先感謝指導教授張志揚教授, 兩年來的指導; 使我對研究主題有一定程度的理解, 使本篇論文可以完成. 其次感謝論文口試委員; 邱煥凱教授, 郭仁財教授與陳正中博士, 對論文內容的建議與意見, 使論文能更加完善.

再來感謝前瞻微波技術實驗室的王侑信學長與微波 CAD 實驗室的林烈全學長, 在量測儀器上的幫忙.

也感謝實驗室的學長與同學, 特別是小谷, 鈞翔, 建育, 慶爺, 梁八, 雞哥, 綸哥, 錞哥, 亭姐與文爺. 感謝我的家人, 媽媽和妹妹; 謝謝大家的支持, 使我能完成碩士學業.

最後僅將本論文獻給我的父親.

Contents

List of Tables

List of Figures

Chapter 1

Introduction

In this chapter , we are going to introduce the importance of microwave / RF filters in modern wireless communication system. Three commercial wireless communication systems, namely, Bluetooth, Zigbee, and Wi-Fi. Moreovr, the basics of coplanar stripline (CPS) will also be introduced.

1.1 The Importance of Microwave- / RF Filters in Modern Wireless Communication System

Recently, communication industry is rising in the global range. Each communication system equips with more and more functions at the same time. Generally, modern wireless communication systems include mobile phone, personal communication system, satellite communication, and wireless area network,..., etc.

Microwave / radio frequency (RF) passive component (such as resistor, capacitor, inductor, filter, and coupler) still takes the most important position in the wireless communication modules. Filter is an important component, and its functions are passing the desired signals and rejecting the undesired one.

According to Fig. 1.1, filter locats in front of the low noise amplifier (LNA) and after the antenna. Passive components take almost 65 percent area of the front-ended circuit in the wireless communication systems, especially antenna and filters. Antenna and filters can not convert to silicon substrate, due to their frequency response characteristic will affect accuracy and quality of whole circuit when processing signals.

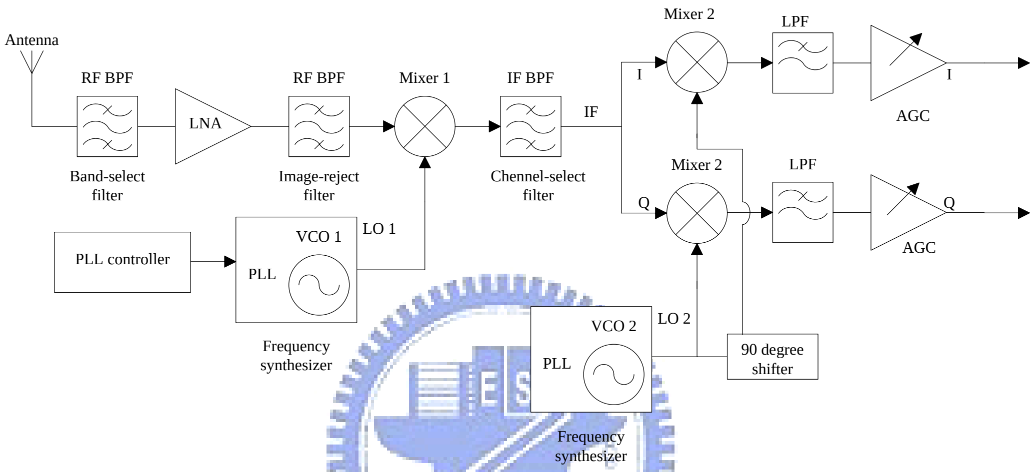

Figure 1.1: Architecture of transceiver system

1.2 Comparison with Bluetooth/ Zigbee/ Wi-Fi

In this section, we introduce three commercial wireless communication systems.

standard	frequency	bandwidth	data rate	outdoor distance
Bluetooth	2.4-2.483 (GHz)	1 (MHz)	1 (Mbps)	1-100 (m)
Zigbee	2.4-2.483 (GHz)	5 (MHz)	256 (Kbps)	10-75 (m)
Wi-Fi	2.4-2.483 (GHz)	20(MHz)	11/54 (Mbps)	32-95 (m)

Table 1.1: Table of comparison between Bluetooth/ Zigbee/ Wi-Fi

Bluetooth is a wireless protocol with short-range communications technology. It utilizes data transmissions over short distances from fixed and/or mobile devices, and causes wireless personal area networks (PANs). It also provides a way to connect and exchange information between devices such as mobile phones, personal computers, printers, GPS receivers, and video game consoles over a secure, globally unlicensed Industrial, Scientific, and Medical (ISM) 2.4 GHz short-range radio frequency bandwidth.

ZigBee is the name of a specification for a suite of high level communication protocols using small, low-power digital radios based on the IEEE 802.15.4 standard for wireless personal area networks (WPANs). The technology is intended to be simpler and cheaper than other WPANs, such as Bluetooth. ZigBee is targeted at radio frequency applications that require a low data rate, long battery life, and secure networking.

Wi-Fi is the trade name for a popular wireless technology used in home networks, mobile phones, video games and more. Wi-Fi is supported by nearly every modern personal computer operating system and most advanced game consoles [1]-[3].

1.3 Basic Concepts of Coplanar Stripline

The coplanar stripline (CPS) was introduced in the mid-1970's [4]-[6] as a transmission medium with the capability to provide uniplanar designs. Its cross sectional is shown in Fig. 1.2 [7], [8]. There are top metal , middle dielectric, and no bottom metal layer. That is the most different portion between CPS and coupled microstripline.

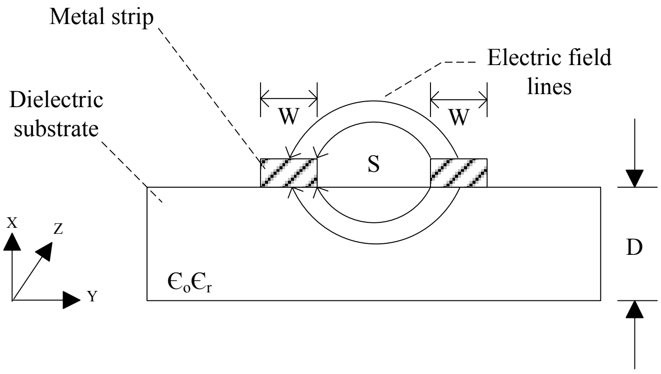

Figure 1.2: Cross section of coplanar stripline

According to the Fig. 1.2. The electromagnetic wave is only propagating on the top metal, which is odd mode excitation. It cause differential input and output, which is better to reject the noise.

It could be regarded as virtual ground in the middle of two stripline of top metal layer, which also considered that electrical-wall or perfect conductor (PEC) there. Furthermore, a CPS can achieve higher characteristic impedances (Z_0 over 150 ohm) than a coplanar waveguide (CPW) and a microstripline by increasing the distance between the two striplines. It only need to analysis half circuit for design whole circuit. CPS has gained a significant momentum in the design and applications of high-density radio-frequency integrated circuits (RFICs) [9].

Besides, many RF components are designed with differential I/O, such as amplifiers, mixers and some of the antennas with symmetric structures. The uniform design of RF components with balanced structure can remove the requirement of unbalance-balance transformation which may cause loss to the system. CPS has the capability to provide excellent propagation characteristics, such as small dispersion and less sensitivity to substrate thickness when appropriately designed. Moreover , this kind of structure is able to provide integration in a high level, efficient in use of wafer area and has great flexibility in design of uniplanar circuits while the via hole or air-bridge is not needed.

Another advantage of this kind of CPS resonator is that the series connection of the stubs are capable of providing high impedance level and increased Q-value which is desirable in certain case of filter design [10]-[12]. The whole system has been reported [13]-[15] with the co-design of filter and antenna, as shown in Fig. 1.3. Furthermore, it has been widely used as interconnects in high-speed digital circuits and integrated electrooptic components.

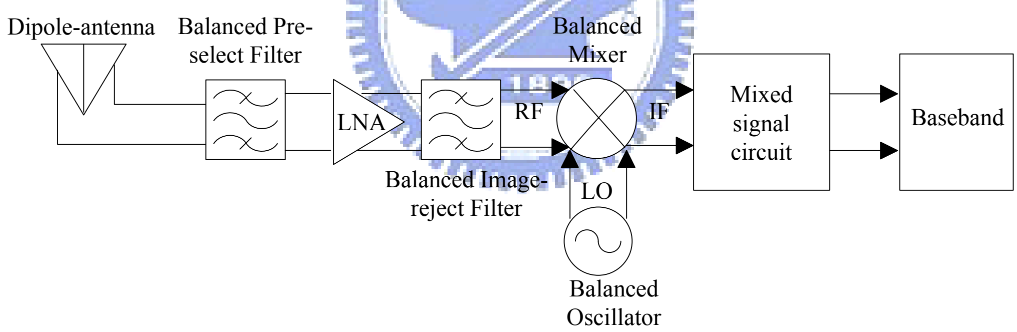

Figure 1.3: Simplified architecture of balanced transceiver system

1.4 Summary

Chapter 1 introduced basic concepts about microwave- / RF filter, commercial wireless communication systems and coplanar striplines. Next chapter will discuss band-pass filter design theory. Chapter 3 introduces the measurement theory about mixed-mode S-parameters and taper transition circuit. Then, chapter 4 shows design examples and its measurement data. The last chapter is conclusion.

Chapter 2

Band-Pass Filter Design Theory

This chapter, we will discuss 4-port scattering parameters of CPS, formulas for band-pass filters with Tchebyshev response, and the analytical design method for band-pass filter. The analytical design procedure includes basic concepts of admittance inverter and impedance inverter, and design procedure flow of a CPS band-pass filter.

2.1 4-port Z-Parameter Analysis of the CPS Circuit

According to the section 1.3, we could analysis a CPS by even mode and odd mode to find its scattering parameters (S-parameters), as shown in Fig. 2.1 and Fig. 2.2. It is a lossless, matched,reciprocal network. θ is electrical length, θ_e is the even mode electrical length, and θ_o is the odd mode electrical length. The input impedances are

$$Z_{short-circuit} = jZ_0 tan\theta \tag{2.1}$$

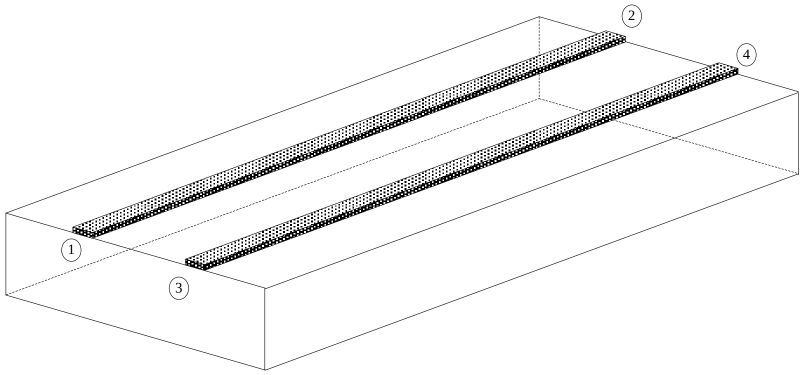

Figure 2.1: Three dimmensional view of CPS for analyzing of 4-port Z-parameters

$$Z_{open-circuit} = -jZ_0 cot\theta \tag{2.2}$$

In Fig. 2.2 (a) to (d), a PMC in the middle of two stripline in even mode excitation and a PEC located between them in odd mode excitation :

$$\begin{aligned} Z_{ee} &= -jZ_e cot(\theta_e/2), \\ Z_{eo} &= -jZ_o cot(\theta_o/2), \\ Z_{oe} &= jZ_e tan(\theta_e/2), \\ Z_{oo} &= jZ_o tan(\theta_o/2), \end{aligned} \tag{2.3}$$

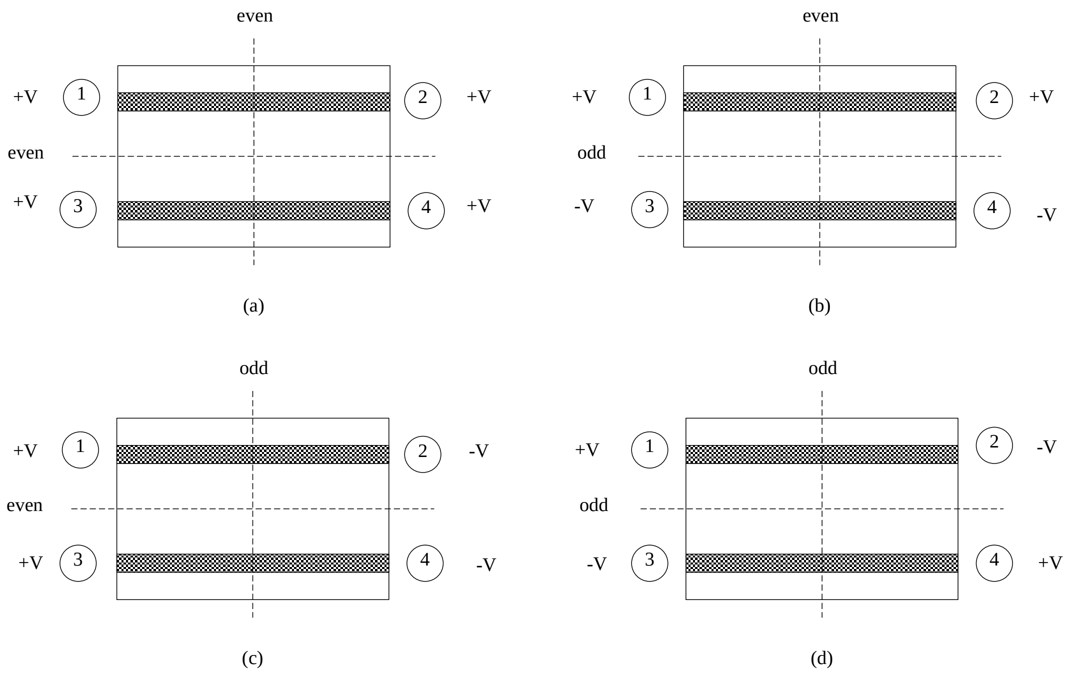

Figure 2.2: Analysis Z-parameters of coplanar stripline for top view(a)even-even(b)even-odd(c)odd-even(d)odd-odd

$$
\begin{aligned}
Z_{11} &= \frac{-j}{2}(Z_e cot\theta_e + Z_o cot\theta_o) \\
Z_{21} &= \frac{-j}{2}(Z_e csc\theta_e + Z_o csc\theta_o) \\
Z_{31} &= \frac{-j}{2}(Z_e cot\theta_e - Z_o cot\theta_o) \\
Z_{41} &= \frac{-j}{2}(Z_e csc\theta_e - Z_o csc\theta_o)
\end{aligned}
\tag{2.4}
$$

as we known:

$$Z_{11} = Z_{22} = Z_{33} = Z_{44}$$

$$Z_{12} = Z_{21} = Z_{34} = Z_{43}$$

$$Z_{13} = Z_{31} = Z_{24} = Z_{42}$$

$$Z_{14} = Z_{41} = Z_{23} = Z_{32}$$

Finally, we can obtain the 4-port Z-parameters:

$$Z = \begin{pmatrix} Z_{11} & Z_{12} & Z_{13} & Z_{14} \\ Z_{21} & Z_{22} & Z_{23} & Z_{24} \\ Z_{31} & Z_{32} & Z_{33} & Z_{34} \\ Z_{41} & Z_{42} & Z_{43} & Z_{44} \end{pmatrix}$$

2.2 Tchebyshev Response and Formula

The transfer function of a filter network is a mathematical description of network response characteristics, namely, a mathematical expression of S_{21}. On many occasions,an amplitude-squared transfer function for a lossless passive filter network is defined as

$$|S_{21}(j\Omega)|^2 = \frac{1}{1 + \epsilon^2 Fn^2(\Omega)} \tag{2.5}$$

where ϵ is a ripple constant, Fn(ϵ) represents a filtering or characteristic function, and Ω is a frequency variable. For our discussion here, it is convenient to let Ω

represent a radian frequency variable of a low-pass prototype filter that has a cutoff frequency at $\Omega = \Omega_c$. For a given transfer function of (2.5), the insertion loss response of the filter, following, can be computed by

$$L_A(\Omega) = 10log\frac{1}{1 + |S_{21}(j\Omega)|^2} \tag{2.6}$$

Since $|S_{11}|^2 + |S_{21}|^2 = 1$ for a lossless, passive 2-port network,the return loss response of the filter can be found

$$L_R(\Omega) = 10log[1 - |S_{21}(j\Omega)|^2](dB) \tag{2.7}$$

The Tchebyshev response exhibits the equal-ripple pass band and maximally flat stop band, as shown in Fig. 2.3.

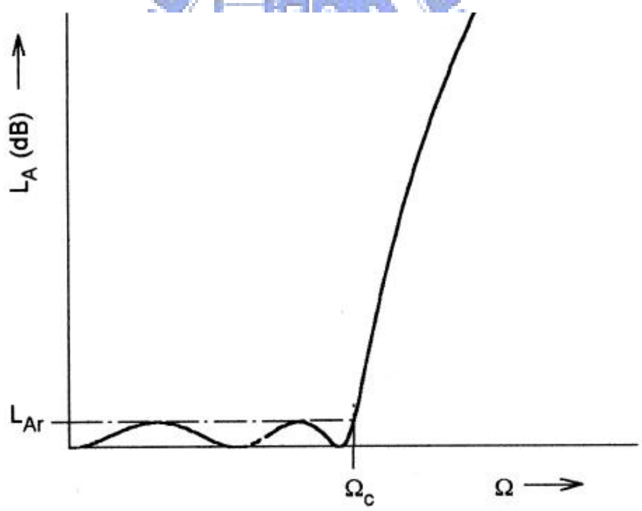

Figure 2.3: Tchebyshev lowpass response

The amplitude-squared transfer function that describes this type of response is

$$|S_{21}(j\Omega)|^2 = \frac{1}{1 + \epsilon^2 Tn^2(\Omega)} \tag{2.8}$$

where the ripple constant ϵ is related to a given pass band ripple L_{Ar} in dB by

$$\epsilon = \sqrt{10^{\frac{L_{Ar}}{10}} - 1} \tag{2.9}$$

Tn(Ω) is a Tchebyshev function of the first kind of order n, which is defined as

$$Tn(\Omega) = \begin{cases} cos(ncos^{-1}(\Omega)) & if|\Omega| \leq 1 \\ cosh(ncosh^{-1}(\Omega)) & if|\Omega| \geq 1 \end{cases} \tag{2.10}$$

Hence, the filters realized from (2.8) are commonly known as Tchebyshev filters. For Tchebyshev low-pass prototype filters have a transfer function given in (2.8) with a pass band ripple L_{Ar} dB and the cutoff frequency $\Omega_c = 1$,the element values for the 2-port networks may be computed by the following formulas:

$$\begin{aligned} g_0 &= 1 \\ a_i &= sin[\frac{(2i-1)\pi}{2N}] \\ b_k &= \gamma^2 + sin^2(\frac{i\pi}{N}) \\ g_1 &= \frac{a_1}{\gamma} \\ g_i &= \frac{4a_{i-1}a_i}{b_{i-1}g_{i-1}} \\ i &= 1, 2, 3, ..., N \end{aligned} \tag{2.11}$$

and

$$g_{N+1} = \begin{cases} coth^2(\frac{\beta}{4}) & ifN \in even \\ 1 & ifN \in odd \end{cases} \tag{2.12}$$

where

$\beta = ln(coth\frac{L_{Ar}}{17.37})$

$\gamma = sinh(\frac{\beta}{2N})$

N is order number

In (2.11) and (2.12), we could find any Tchebyshev low-pass prototype element values for any ripple value [16], [17].

2.3 Analytical Method

2.3.1 Basic Concepts of Admittance Inverter and Impedance Inverter

In this section, we consider the basic admittance-inverter and impedance-inverter model for filter synthesizing [16], [17].

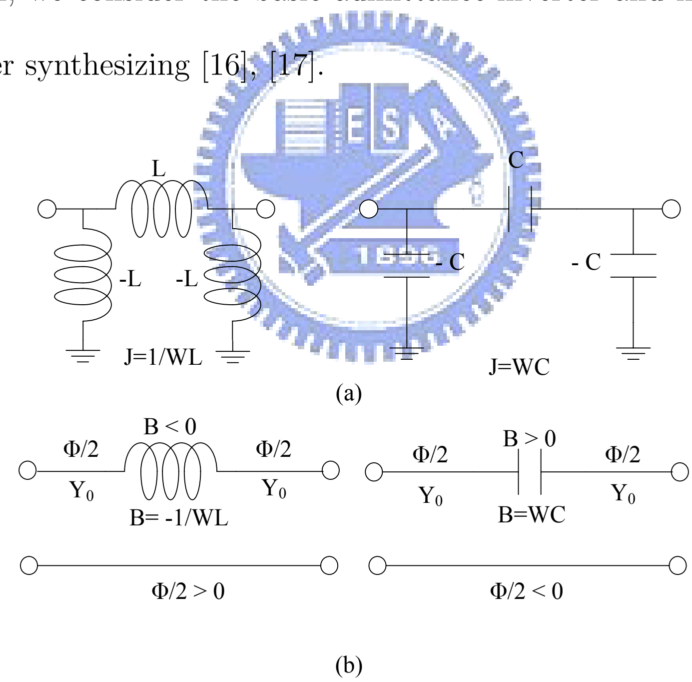

Figure 2.4: Admittance inverter (J inverter)(a) lumped element (b) transmission line

First, there are two different types of the admittance inverter (J inverter) model at Fig.2.4 (a) and (b). One is suited for lumped element and the other is suited for transmission line. The formulas for Fig. 2.4(b) are given as:

$$
\begin{aligned}
J &= Y_0 tan|\frac{\Phi}{2}|, \\
\Phi &= -tan^{-1}(\frac{2B}{Y_0}), \\
|\frac{B}{Y_0}| &= \frac{(\frac{J}{Y_0})}{1-(\frac{J}{Y_0})^2},
\end{aligned}
\tag{2.13}
$$

Their equivalent model for admittance inverter (J inverter) is at Fig. 2.5.

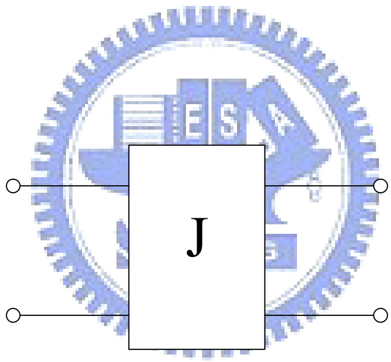

Figure 2.5: Equivalent model for J inverter

By duality, there also have two different types of the Impedance inverter (K inverter) model at Fig.2.5 (a) and (b). One is for lumped element, and the other is for transmission line, too. Fig. 2.7 is their equivalent circuit for Impedance inverter (K inverter). The design formular are shown below in (2.14).

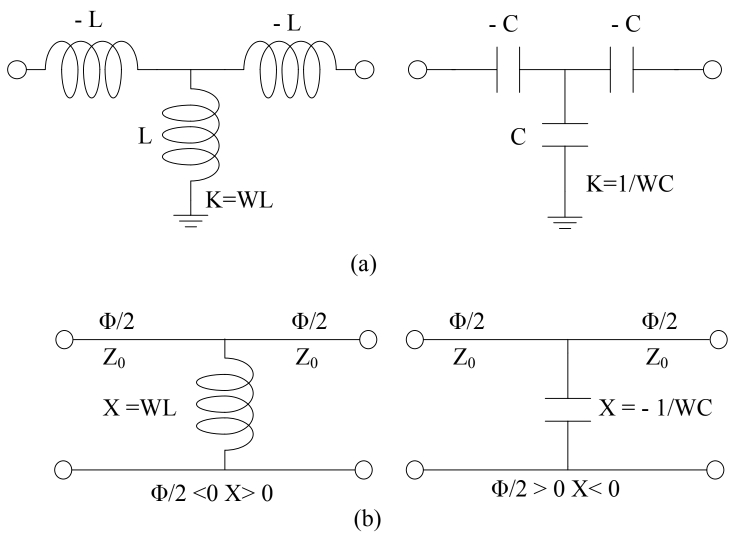

Figure 2.6: Impedance inverter (K inverter)(a) lumped element (b) transmission line

$$K = Z_0 tan|\frac{\Phi}{2}|,$$
$$\Phi = -tan^{-1}(\frac{2X}{Z_0}), \tag{2.14}$$
$$|\frac{X}{Z_0}| = \frac{(\frac{K}{Z_0})}{1-(\frac{K}{Z_0})^2},$$

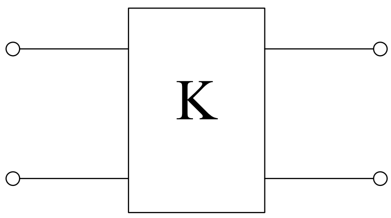

Figure 2.7: Equivalent Model for K inverter

All of them can be proved by Y matrix and Z matrix [18].

$$
\begin{aligned}
Y &= \begin{pmatrix} Y_{11} & Y_{12} \\ Y_{21} & Y_{22} \end{pmatrix} \\
Z &= \begin{pmatrix} Z_{11} & Z_{12} \\ Z_{21} & Z_{22} \end{pmatrix}
\end{aligned}
\tag{2.15}
$$

They are useful for filter design which $\frac{\Phi}{2}$ can be absorbed into resonator' s electrical length in (2.13) and (2.14). Examples electrical length are shown in Fig. 2.8 and Fig. 2.9, where 180^o means $\lambda/2$ resonator.

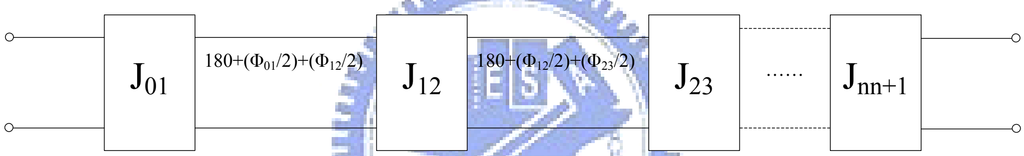

Figure 2.8: Diagram of J inverter filter

The formulas for J inverter filter as shown in Fig. 2.8 are depicted below.

$$
\begin{aligned}
J_{01} &= \sqrt{\frac{G_S b_{1r} \Delta}{g_0 g_1}} \\
J_{jj+1} &= \Delta \sqrt{\frac{b_{jr} b_{j+1r}}{g_j g_{j+1}}} \\
J_{nn+1} &= \sqrt{\frac{G_L b_{nr} \Delta}{g_n g_{n+1}}} \\
G_S &= \frac{1}{Z_0} = G_L
\end{aligned}
\tag{2.16}
$$

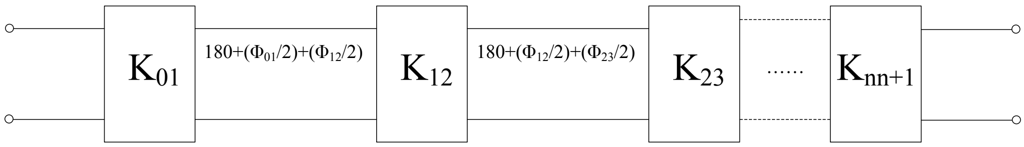

Figure 2.9: Diagram of K inverter filter

The design formulas for a filter with K inverters are shown in the following.

$$
\begin{aligned}
K_{01} &= \sqrt{\frac{R_S x_{1r} \Delta}{g_0 g_1}} \\
K_{jj+1} &= \Delta \sqrt{\frac{x_{jr} x_{j+1r}}{g_j g_{j+1}}} \\
K_{nn+1} &= \sqrt{\frac{R_L x_{nr} \Delta}{g_n g_{n+1}}} \\
R_S &= R_L = Z_0
\end{aligned}
\tag{2.17}
$$

In (2.16) and (2.17), the b_{jr} is susceptance slope parameter of the j-th shunt resonance, Δ is fractional bandwidth, use lower case latter. X_{jr} is reactance slope parameter of the j-th series resonance, and g_j is the Tchebyshev low-pass prototype element values, which could be obtained in (2.11). By their definition:

$$
\begin{aligned}
b_j &= \frac{\omega_0}{2} \frac{dB_j(\omega)}{d\omega}|_{\omega=\omega_0} \\
x_j &= \frac{\omega_0}{2} \frac{dX_j(\omega)}{d\omega}|_{\omega=\omega_0}
\end{aligned}
$$

We could obtain:

$$
\begin{aligned}
b_j &= \begin{cases} \frac{\pi}{2} Y_o & , \frac{\lambda}{2} - resonator \\ \frac{\pi}{4} Y_o & , \frac{\lambda}{4} - resonator \end{cases} \\
x_j &= \begin{cases} \frac{\pi}{2} Z_o & , \frac{\lambda}{2} - resonator \\ \frac{\pi}{4} Z_o & , \frac{\lambda}{4} - resonator \end{cases}
\end{aligned} \tag{2.18}
$$

2.3.2 Novel J and K Inverter for CPS

As section 2.1, we already known that CPS could be analyzed by half circuit analysis [19]-[22]. In this section, we inductre J and K inverter equivalent model for filter as shown in Fig. 2.10. The half-circuit of the CPS J and K inverter are also shown in the figure.

From Fig. 2.10 (a) to (c), they can be modeling as the equivalent model of CPS' half-circuit, which also could be proved by (2.15).

The capacitance Cg and Cp that appear in the equivalent π-network as shown in Fig. 2.10(a)and (b) may be determined as Fig. 2.11(a) and (b) by using the EM-simulator, and also the inductance Ls and Lp that appear in the equivalent T-network in Fig. 2.10(c) as Fig. 2.12(a) and (b). In Fig. 2.12, (a) is size-I and (b)is size-II, which W1 of (a) is smaller than (b), and length of (a) is bigger than (b).

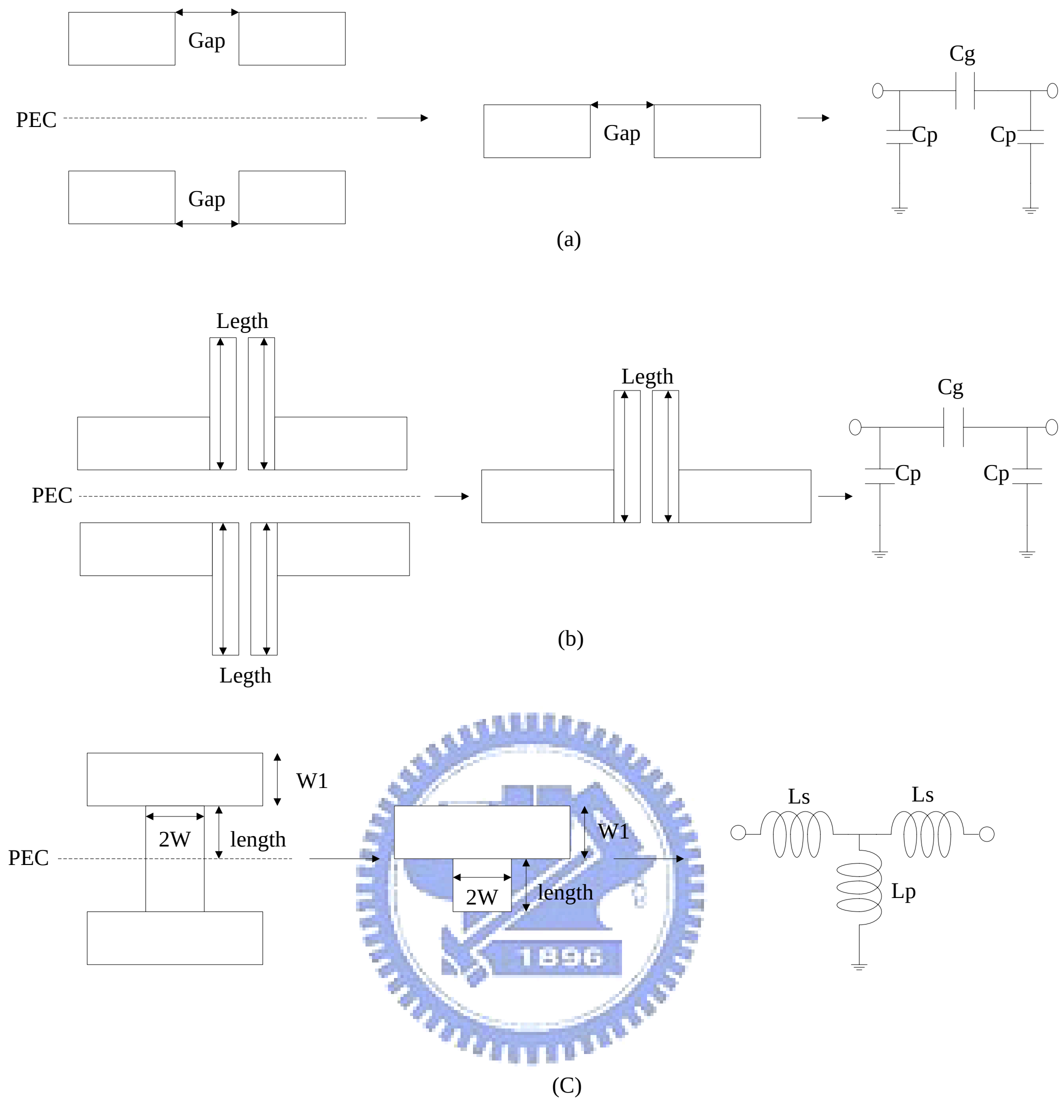

Figure 2.10: Proposed J and K inverter for CPS (a)J inverter (b)J inverter (c)K inverter

$$C_g = -\frac{I_m(Y_{21})}{\omega_0}$$

$$C_p = \frac{I_m(Y_{11} + Y_{21})}{\omega_0}$$

$$L_s = \frac{I_m(Z_{21})}{\omega_0}$$

$$L_p = \frac{I_m(Z_{11} - Z_{21})}{\omega_0}$$

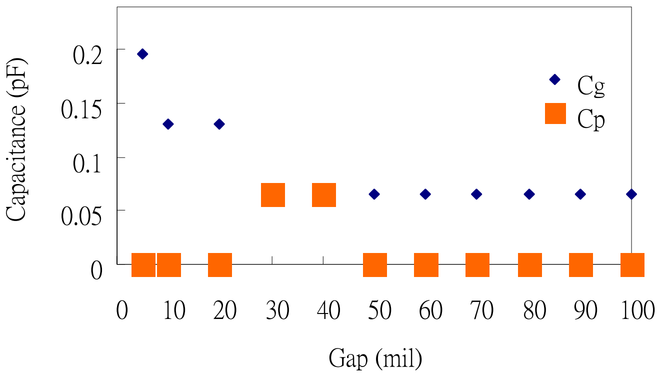

(a)

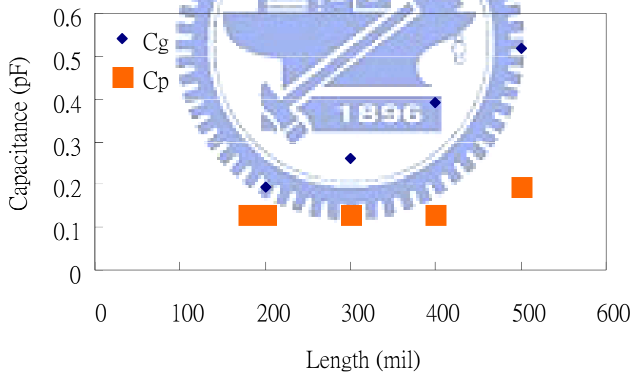

(b)

Figure 2.11: Capacitance versus physical dimmension in(a)Gap(b)Lengh

According to Fig. 2.11 and 2.12 , we could find the values for filter design, which we need. And then, use (2.19) and (2.20) to calculate the initial guess. We will use

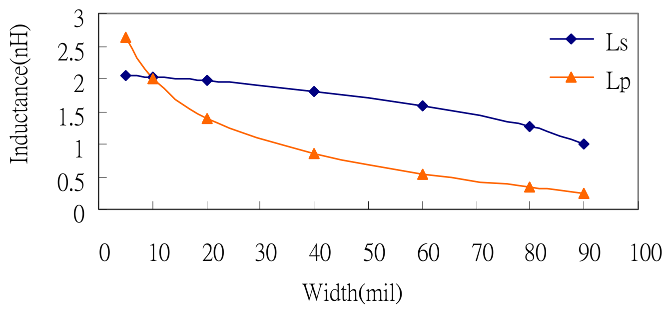

(a)

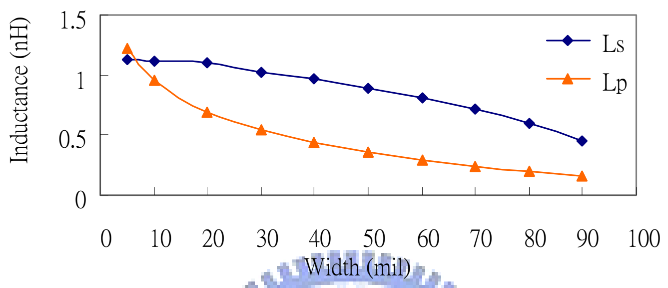

(b)

Figure 2.12: Inductance versus physical dimmension in (a)size-I (b)size-II

them in chapter 4.

$$\begin{aligned}
\theta_j &= \pi - \frac{1}{2}[tan^{-1}(\frac{2B_{j-1j}}{Y_0}) + tan^{-1}(\frac{2B_{jj+1}}{Y_0})](radians) \\
C_g^{jj+1} &= \frac{B_{jj+1}}{\omega_0} \\
l_j &= \frac{\lambda_{g0}}{2\pi}\theta_j - \Delta_j^{e1} - \Delta_j^{e2} \\
\Delta_j^{e1} &= \frac{\omega_0 C_p^{j-1j}}{Y_0}\frac{\lambda_{g0}}{2\pi} \\
\Delta_j^{e2} &= \frac{\omega_0 C_p^{jj+1}}{Y_0}\frac{\lambda_{g0}}{2\pi}
\end{aligned} \tag{2.19}$$

By duality, there also have:

$$
\begin{aligned}
\theta_j &= \pi - \frac{1}{2}[tan^{-1}(\frac{2X_{j-1j}}{Z_0}) + tan^{-1}(\frac{2X_{jj+1}}{Z_0})](radians) \\
L_p^{jj+1} &= \frac{X_{jj+1}}{\omega_0} \\
l_j &= \frac{\lambda_{g0}}{2\pi}\theta_j - \Delta_j^{e1} - \Delta_j^{e2} \qquad (2.20) \\
\Delta_j^{e1} &= \frac{\omega_0 L_s^{j-1j}}{Y_0}\frac{\lambda_{g0}}{2\pi} \\
\Delta_j^{e2} &= \frac{\omega_0 L_s^{jj+1}}{Y_0}\frac{\lambda_{g0}}{2\pi}
\end{aligned}
$$

where $\omega_0 = 2\pi f_0$, and f_0 is center frequency. If changes the π to $\pi/2$ in (2.19)-(2.20), we can obtained the formulas for $\lambda/4$ resonators cases.

2.3.3 Design Procedure Flow Chart

After knowing the filter parameters for Tchebyshev response and formulas for J / K inverters, we follow the design flow shown in Fig. 2.13 to complete the filter design. First, we have to define band-pass filter' s center frequency, fractional bandwidth, order, and ripple level. Second, calculate its low-pass prototype element values to obtain J inverter or K inverter values. Third, use analytical method to get the initial design of the filter and fine tune it on EM-simulator. Finally, implement circuit and measure it.

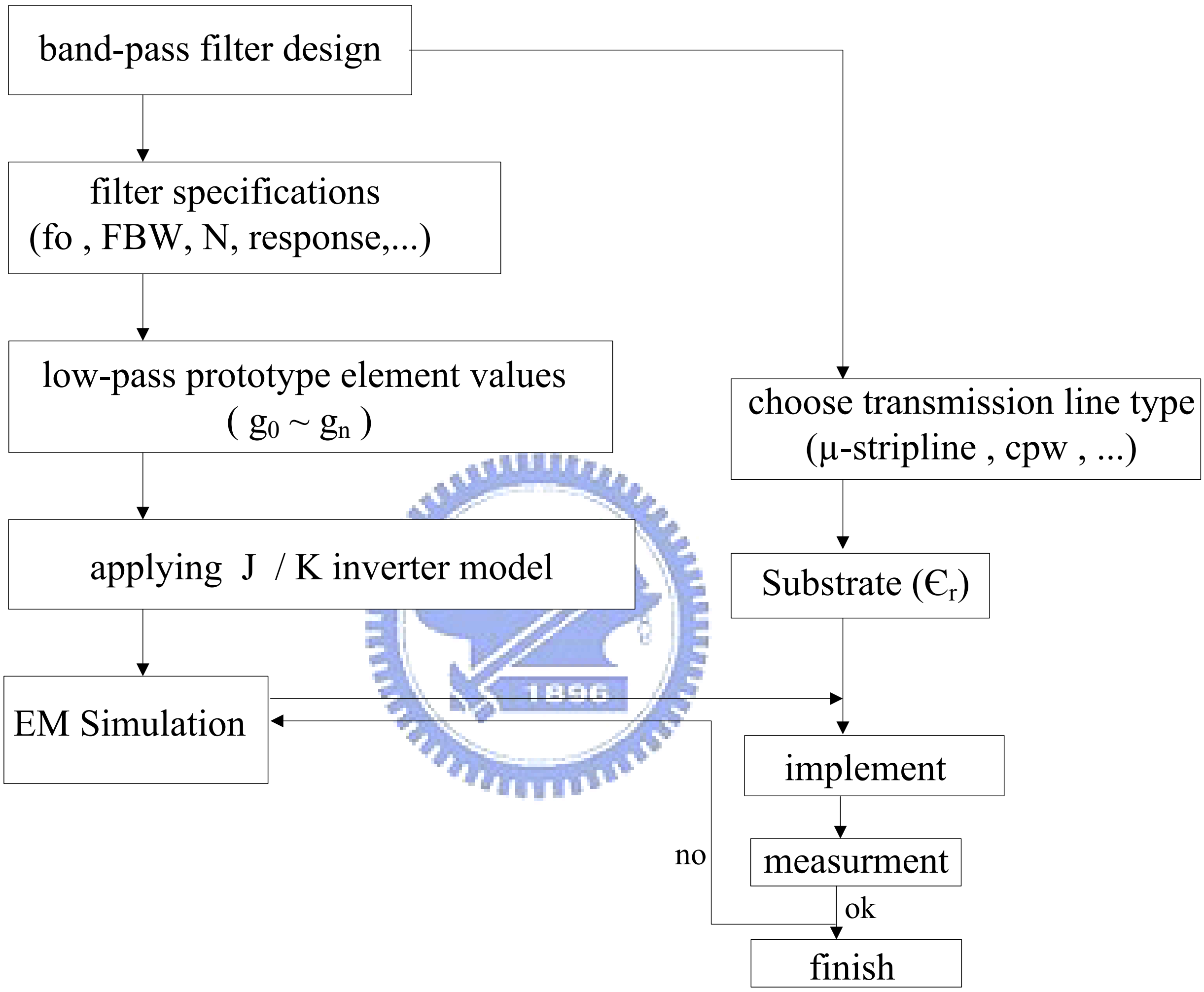

Figure 2.13: Diagram of design procedure flow

Chapter 3

Measurement Theory and Taper Transition Circuit

In this chapter, we will disscuss the measurement of mixed-mode S-parameters. And then compare three types of taper transition circuits for measurement.

3.1 Mixed-mode S-Parameters

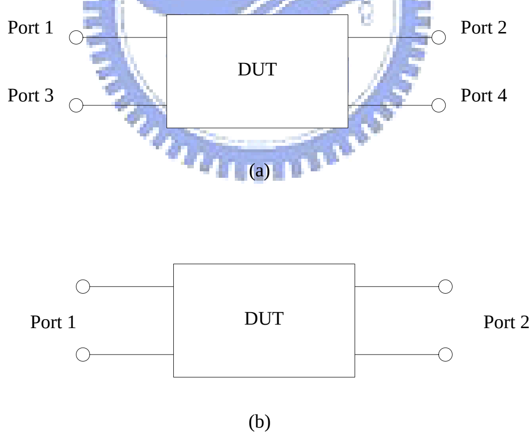

Figure 3.1: (a)Diagram of single-ended 4-port DUT (b)Diagram of differential 2-port DUT

An S-parameter is defined as the ratio of two normalized power waves, that is the response divided by the stimulus. A full S-matrix (3.1) describes every possible combination of a response divided by a stimulus. The matrix is arranged in such a way that each column represents a particular stimulus condition, and each row represents a particular response condition. The standard 4-port S-parameters matrix is given below.

$$\begin{pmatrix} b_1 \\ b_2 \\ b_3 \\ b_4 \end{pmatrix} = \begin{pmatrix} S_{11} & S_{12} & S_{13} & S_{14} \\ S_{21} & S_{22} & S_{23} & S_{24} \\ S_{31} & S_{32} & S_{33} & S_{34} \\ S_{41} & S_{42} & S_{43} & S_{44} \end{pmatrix} \begin{pmatrix} a_1 \\ a_2 \\ a_3 \\ a_4 \end{pmatrix} \tag{3.1}$$

Or $B_{std} = S_{std}A_{std}$, where B_{std}, and A_{std} are column vectors correspondes incident outgoing waves respectivly. And S_{std} is the standard 4-port S-parameters matrix. They are shown in (3.2) and (3.3) respectivly .

$$B_{std} = \begin{pmatrix} b_1 \\ b_2 \\ b_3 \\ b_4 \end{pmatrix} ; A_{std} = \begin{pmatrix} a_1 \\ a_2 \\ a_3 \\ a_4 \end{pmatrix} \tag{3.2}$$

$$S_{std} = \begin{pmatrix} S_{11} & S_{12} & S_{13} & S_{14} \\ S_{21} & S_{22} & S_{23} & S_{24} \\ S_{31} & S_{32} & S_{33} & S_{34} \\ S_{41} & S_{42} & S_{43} & S_{44} \end{pmatrix} \tag{3.3}$$

For a balanced device, differential and common mode voltages and currents can be defined on each balanced port. Differential and common mode impedances can also be defined. A block diagram of a 2-port differential device-under-test (DUT) is shown in Fig. 3.1(b). A mixed-mode S matrix in (3.4) can be organized in a way similar to the single-ended S-matrix, where each column (row) represents a different stimulus (response) condition. The mode information as well as port information must be included in the mixed-mode S matrix.

$$\begin{pmatrix} b_{d1} \\ b_{d2} \\ b_{c1} \\ b_{c2} \end{pmatrix} = \begin{pmatrix} S_{d1d1} & S_{d1d2} & S_{d1c1} & S_{d1c2} \\ S_{d2d1} & S_{d2d2} & S_{d2c1} & S_{d2c2} \\ S_{c1d1} & S_{c1d2} & S_{c1c1} & S_{c1c2} \\ S_{c2d1} & S_{c2d2} & S_{c2c1} & S_{c2c2} \end{pmatrix} \begin{pmatrix} a_{d1} \\ a_{d2} \\ a_{c1} \\ a_{c2} \end{pmatrix} \tag{3.4}$$

S_{didj} and S_{cicj} (i, j=1, 2) are the differential mode and common mode S-parameters respectively. S_{dicj} and S_{cicj} (i, j=1, 2) are the mode-conversion/ cross mode S-parameters. The parameters S_{didj} (i, j=1, 2) in the upper-left corner of the mixed-mode S-matrix (3.4) describe the performance with a differential stimulus and differential response. S_{dicj} (S_{cidj}) (i, j=1, 2) describes the conversion of common mode (differential mode) waves to differential mode (common mode) waves.

The mixed-mode S-parameters in (3.4) can be transformed to standard 4-port S-parameters (3.3). Consider nodes 1 and 2 in Fig. 3.1(a) as a single differential port, and nodes 3 and 4 as another differential port . The relations between the response and stimulus of standard-mode and mixed-mode are shown in (3.5) and (3.6). Where a_i and b_i (i=1 to 4) are the waves measured at ports 1-4 in Fig. 3.1(a).

$$\begin{aligned} a_{d1} &= \tfrac{1}{\sqrt{2}}(a_1 - a_3) \\ a_{c1} &= \tfrac{1}{\sqrt{2}}(a_1 + a_3) \\ b_{d1} &= \tfrac{1}{\sqrt{2}}(b_1 - b_3) \\ b_{c1} &= \tfrac{1}{\sqrt{2}}(b_1 + b_3) \end{aligned} \tag{3.5}$$

$$\begin{aligned} a_{d2} &= \tfrac{1}{\sqrt{2}}(a_2 - a_4) \\ a_{c2} &= \tfrac{1}{\sqrt{2}}(a_2 + a_4) \\ b_{d2} &= \tfrac{1}{\sqrt{2}}(b_2 - b_4) \\ b_{c2} &= \tfrac{1}{\sqrt{2}}(b_2 + b_4) \end{aligned} \tag{3.6}$$

(3.7)-(3.12) gives the transformation between standard and mixed-mode S-matrices.

$$A_{mm} = MA_{std} = \begin{pmatrix} a_{d1} \\ a_{d2} \\ a_{c1} \\ a_{c2} \end{pmatrix} = \frac{1}{\sqrt{2}} \begin{pmatrix} 1 & 0 & -1 & 0 \\ 0 & 1 & 0 & -1 \\ 1 & 0 & 1 & 0 \\ 0 & 1 & 0 & 1 \end{pmatrix} \begin{pmatrix} a_1 \\ a_2 \\ a_3 \\ a_4 \end{pmatrix} \tag{3.7}$$

$$B_{mm} = MB_{std} = \begin{pmatrix} b_{d1} \\ b_{d2} \\ b_{c1} \\ b_{c2} \end{pmatrix} = \frac{1}{\sqrt{2}} \begin{pmatrix} 1 & 0 & -1 & 0 \\ 0 & 1 & 0 & -1 \\ 1 & 0 & 1 & 0 \\ 0 & 1 & 0 & 1 \end{pmatrix} \begin{pmatrix} b_1 \\ b_2 \\ b_3 \\ b_4 \end{pmatrix} \tag{3.8}$$

$$M = \frac{1}{\sqrt{2}} \begin{pmatrix} 1 & 0 & -1 & 0 \\ 0 & 1 & 0 & -1 \\ 1 & 0 & 1 & 0 \\ 0 & 1 & 0 & 1 \end{pmatrix} \tag{3.9}$$

$$M^{-1} = \frac{M^{\star}}{|M|} = \frac{1}{\sqrt{2}} \begin{pmatrix} 1 & 0 & -1 & 0 \\ 0 & 1 & 0 & -1 \\ 1 & 0 & 1 & 0 \\ 0 & 1 & 0 & 1 \end{pmatrix} = M^T \tag{3.10}$$

where M is the conversion matrix.

$$B_{mm} = S_{mm}A_{mm} = \begin{pmatrix} b_{d1} \\ b_{d2} \\ b_{c1} \\ b_{c2} \end{pmatrix} = \begin{pmatrix} S_{d1d1} & S_{d1d2} & S_{d1c1} & S_{d1c2} \\ S_{d2d1} & S_{d2d2} & S_{d2c1} & S_{d2c2} \\ S_{c1d1} & S_{c1d2} & S_{c1c1} & S_{c1c2} \\ S_{c2d1} & S_{c2d2} & S_{c2c1} & S_{c2c2} \end{pmatrix} \begin{pmatrix} a_{d1} \\ a_{d2} \\ a_{c1} \\ a_{c2} \end{pmatrix} \tag{3.11}$$

Use (3.8), (3.7) to substitute (3.11) which can be obtained:

$$MB_{std} = S_{mm}A_{mm}$$

$$B_{std} = S_{std}A_{std}$$

By multipling A_{std}^{-1} which can be obtained:

$$MS_{std}A_{std} = S_{mm}MA_{std}$$

$$MS_{std}A_{std}A_{std}^{-1} = S_{mm}MA_{std}A_{std}^{-1}$$

Here, I=$A_{std}A_{std}^{-1}$ and do it against with M matrix which can be written:

$$MS_{std} = S_{mm}M$$

$$MS_{std}M^{-1} = S_{mm}MM^{-1}$$

At last:

$$S_{mm} = MS_{std}M^{-1} = \begin{pmatrix} S_{dd} & S_{dc} \\ S_{cd} & S_{cc} \end{pmatrix}$$

where

$$\begin{aligned}
S_{dd} &= \frac{1}{2}\begin{pmatrix} S_{11} - S_{13} - S_{31} + S_{33} & S_{12} - S_{14} - S_{32} + S_{34} \\ S_{21} - S_{23} - S_{41} + S_{43} & S_{22} - S_{24} - S_{42} + S_{44} \end{pmatrix} \\
S_{dc} &= \frac{1}{2}\begin{pmatrix} S_{11} + S_{13} - S_{31} - S_{33} & S_{12} + S_{14} - S_{32} - S_{34} \\ S_{21} + S_{23} - S_{41} - S_{43} & S_{22} + S_{24} - S_{42} - S_{44} \end{pmatrix} \\
S_{cd} &= \frac{1}{2}\begin{pmatrix} S_{11} - S_{13} + S_{31} - S_{33} & S_{12} - S_{14} + S_{32} - S_{34} \\ S_{21} - S_{23} + S_{41} - S_{43} & S_{22} - S_{24} + S_{42} - S_{44} \end{pmatrix} \\
S_{cc} &= \frac{1}{2}\begin{pmatrix} S_{11} + S_{13} + S_{31} + S_{33} & S_{12} + S_{14} + S_{32} + S_{34} \\ S_{21} + S_{23} + S_{41} + S_{43} & S_{22} + S_{24} + S_{42} + S_{44} \end{pmatrix}
\end{aligned} \tag{3.12}$$

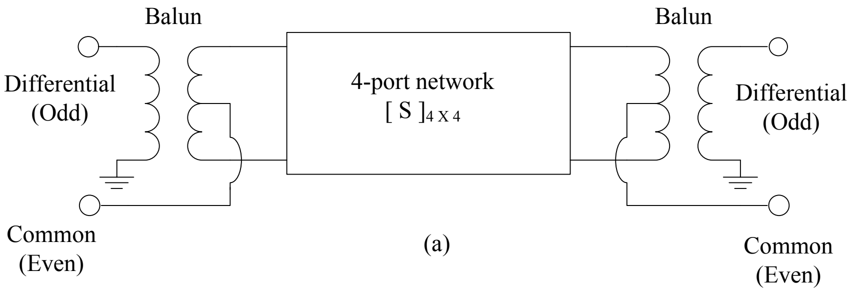

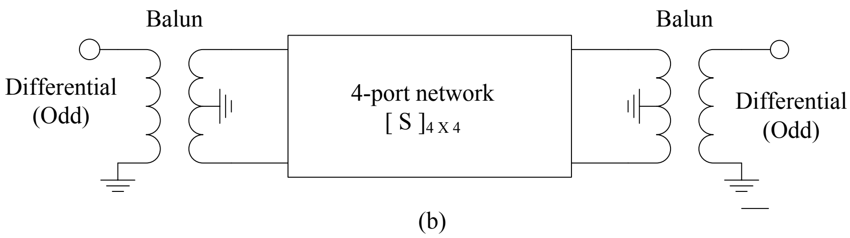

Figure 3.2: (a)Mixed-mode S-parameters (b)Differential S-parameters

As obtained 4-port Z-parameters of CPS in (2.5), and then to extract the mixed-mode S-parameters by (3.12). Actually, the method to find mixed-mode S-parameters by using a balun in Fig. 3.2(a) is identical to make basis transformation mathematically [23]-[25]. In Fig. 3.2(b), it is a test set-up to measure differential mode S-matrix of a DUT.

3.2 Taper Transition Circuits

In this section, three types of transition circuit are introduced and compared for measurement of a CPS line. All circuit are designed with RT/Duroid 4003 substrate with dielectric constant of 3.58 and thickness of 20 mil.

3.2.1 Type-I Transition Circuit

Type-I, which is shown in Fig. 3.3, considers only couple line effect. The simulation results about S_{d1d1} S_{d2d1} are shown in Fig. 3.4.

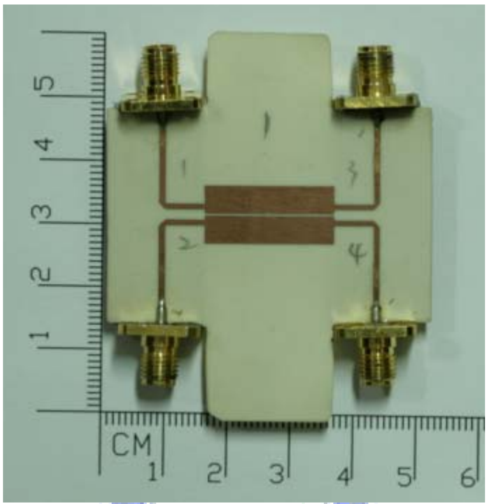

Figure 3.3: Circuit photo of type-I

In addition, its common to common response is shown in Fig. 3.6.

3.2.2 Type-II Transition Circuit

Type-II transition circuit is shown in Fig. 3.7, where the taper portion is added. As shown in the figure, the input microstripline line has couple effect. The simulated and measured performances are depicted in Fig. 3.8 and 3.9. Fig. 3.10 shows the common mode to common mode S-parameters.

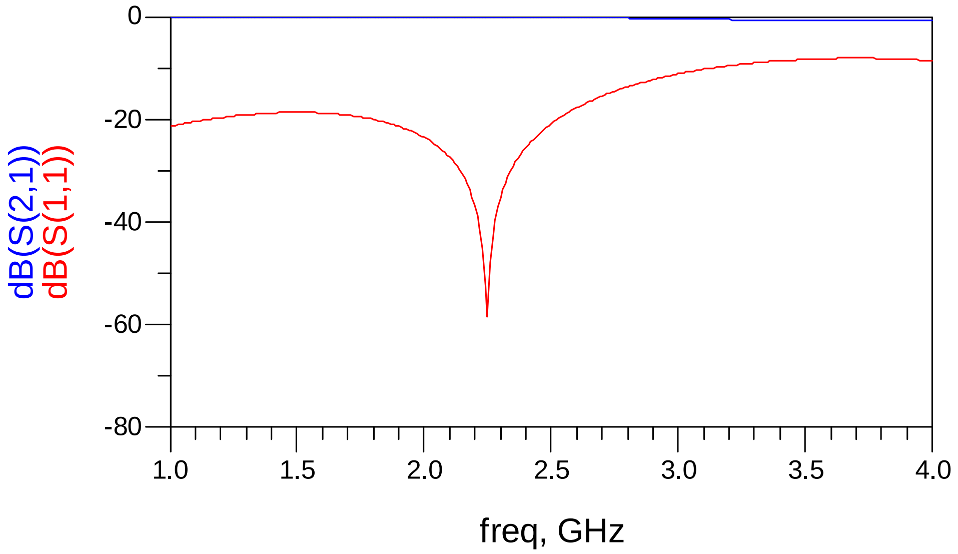

Figure 3.4: Narrow band differential mode simulation result

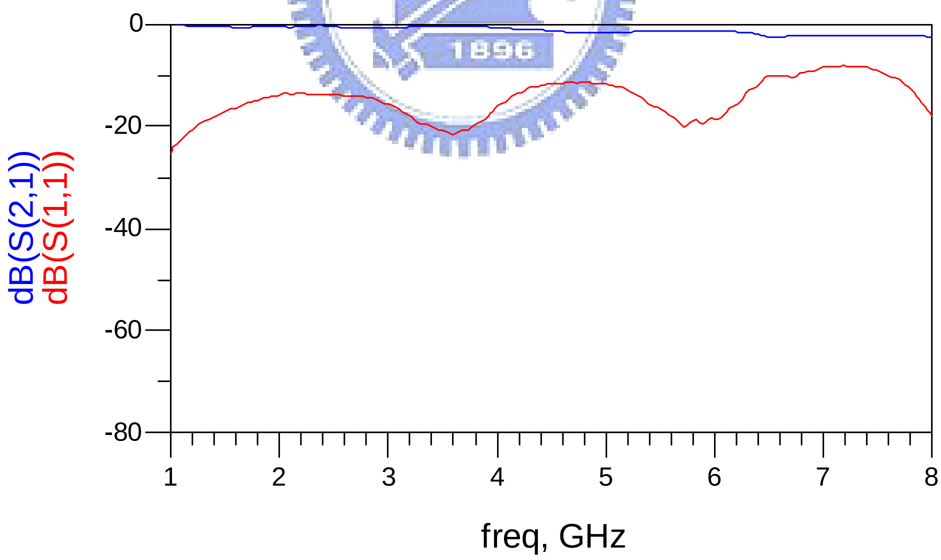

Figure 3.5: broad band differential mode measurement result

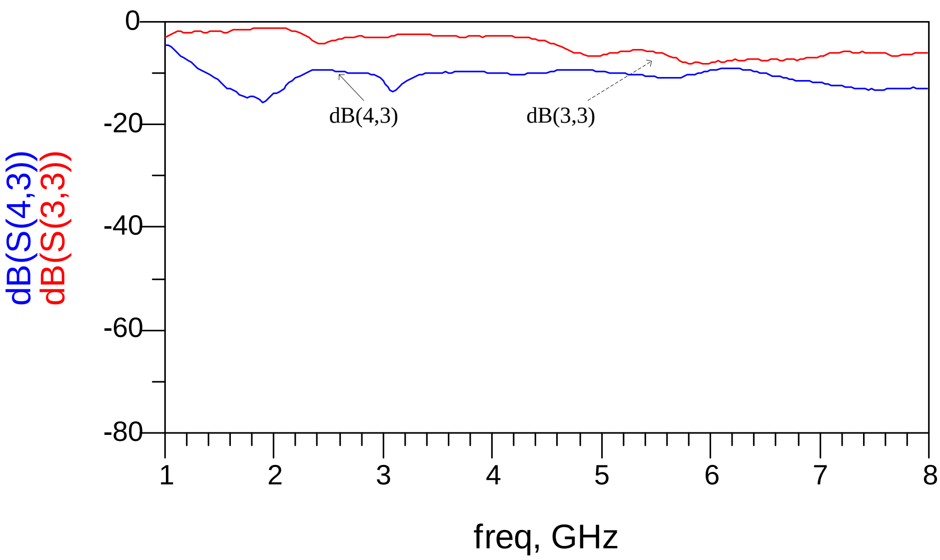

Figure 3.6: Broad band common mode measurement result

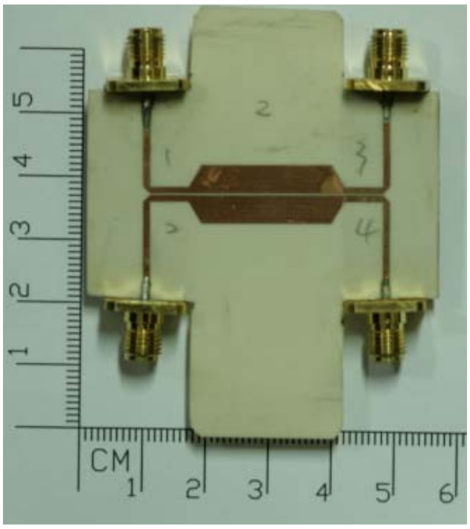

Figure 3.7: Circuit photo of type-II

3.2.3 Type-III Transition Circuit

Type-III transition circuit is shown in Fig. 3.11. Not only a taper line portion is added, but also the decreasing of the coupling effect is taken into account. And it is

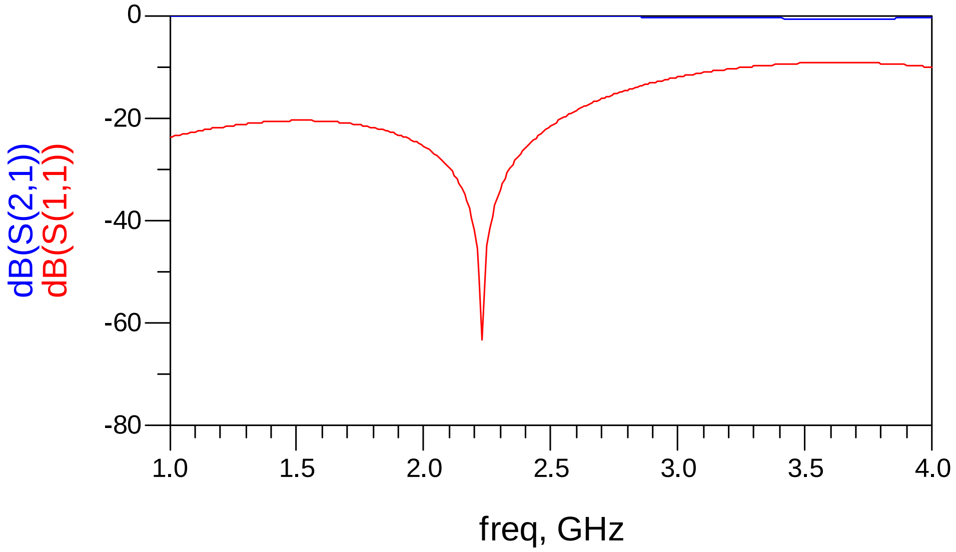

Figure 3.8: Narrow band differential mode simulation result

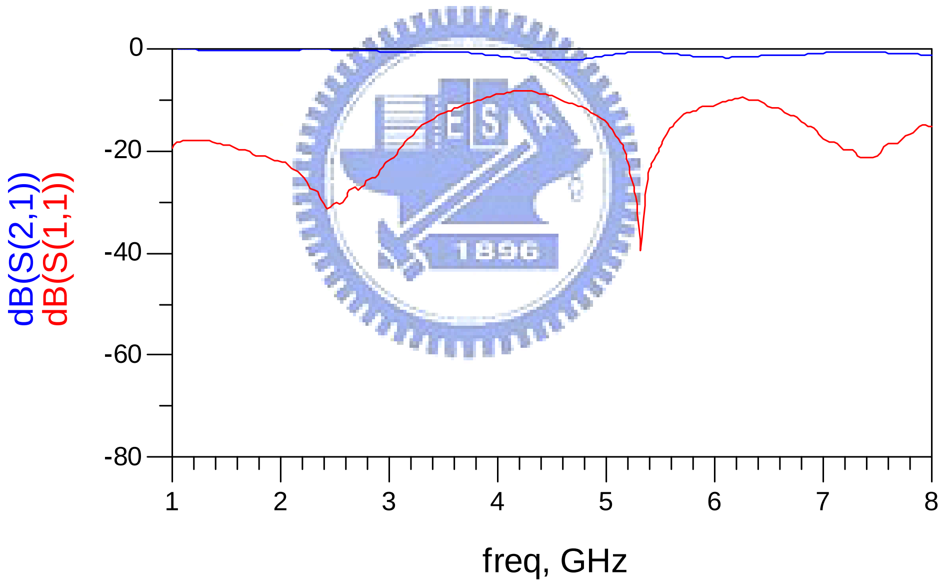

Figure 3.9: Broad band differential mode measurement result

the best of all three types of transition circuit. The type-III transition will be used in chapter 4 for measuring of proposed CPS filters. The simulated and measured

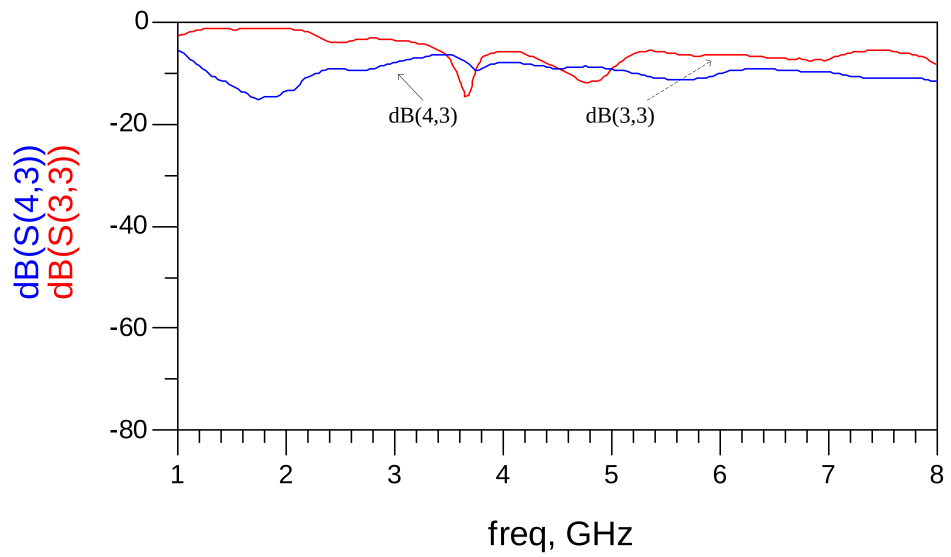

Figure 3.10: Broad band common mode measurement result

performances are depicted in Fig. 3.12-3.14.

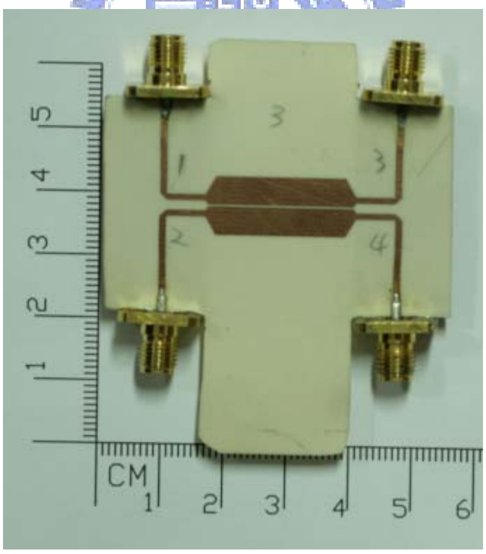

Figure 3.11: Circuit photo of type-III

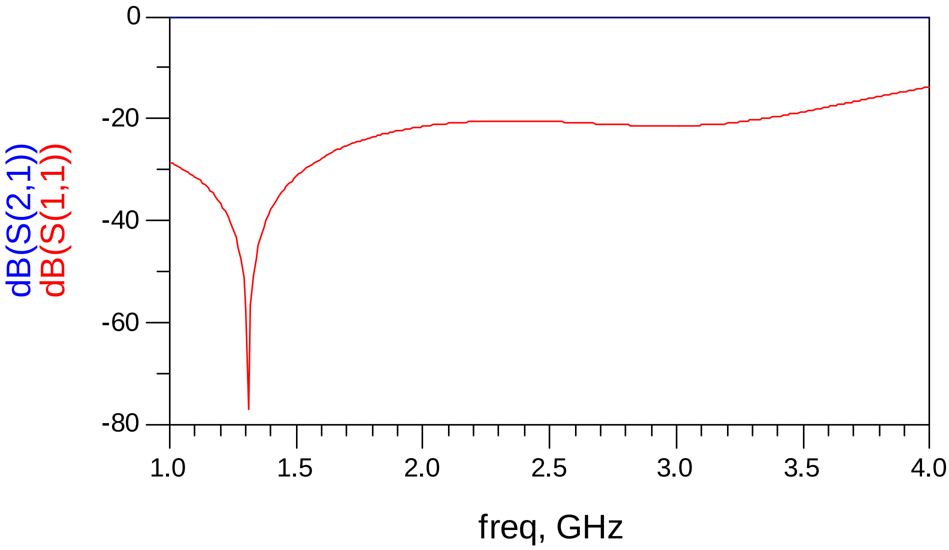

Figure 3.12: Narrow band differential mode simulation result

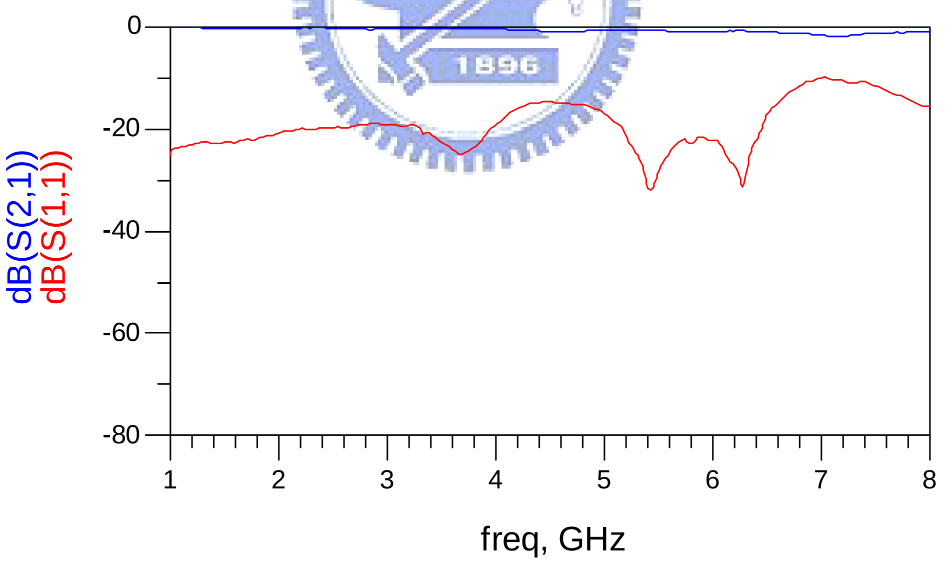

Figure 3.13: Broad band differential mode measurment result

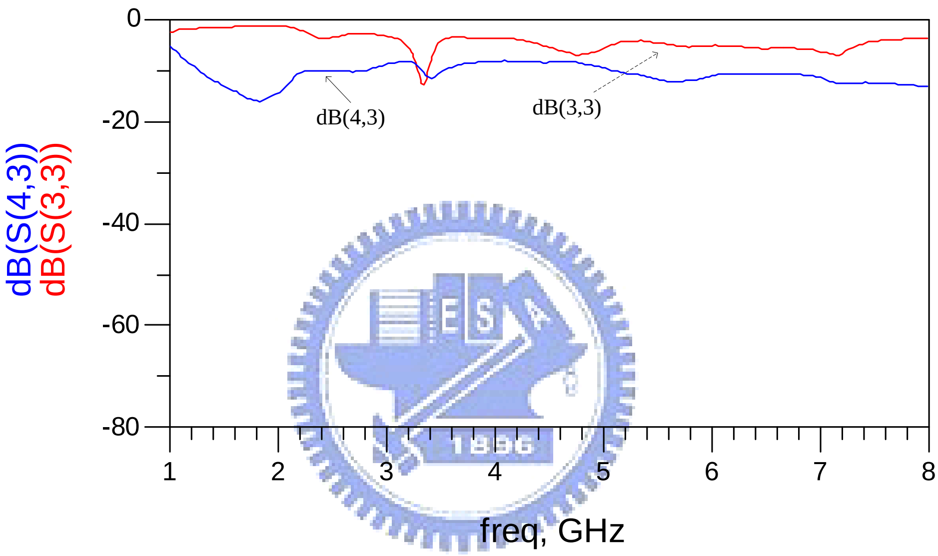

Figure 3.14: Broad band common mode measurment result

Chapter 4

Design Example and Measurement Data

In the previous chapters we have already known the design formulas and procedures for designing a CPS filter, and the measurement techniques have also been discussed in detail in chapter 3. In this chapter, we show a few design examples and their simulated and measured data. All circuit are designed with RT/Duroid 4003 substrate with dielectric constant of 3.58 and thickness of 20 mil.

4.1 Second Order Band-Pass Filter

The ideal half circuit model is shown in Fig. 4.1. We can find the ideal response as shown in Fig. 4.2 by (2.11)-(2.14), and also can obtain the equivalent circuit as shown in Fig. 4.3. Its center frequency f_0 is 2.45GHz, and fractional bandwidth Δ is 5 percent.

Then, use Fig. 2.11 and Fig. 2.12, (2.19), and (2.20) to calculate the initial design. The EM simulated response is depicted in Fig. 4.4, which shown center

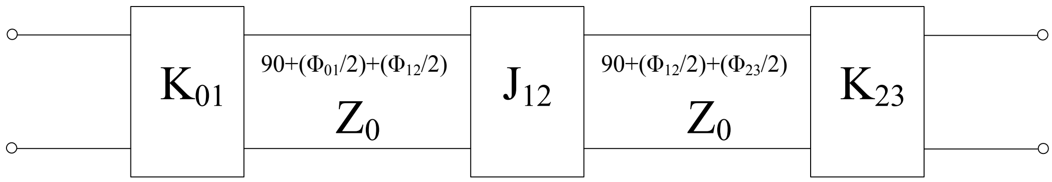

Figure 4.1: Half circuit model of a second order band-pass filter

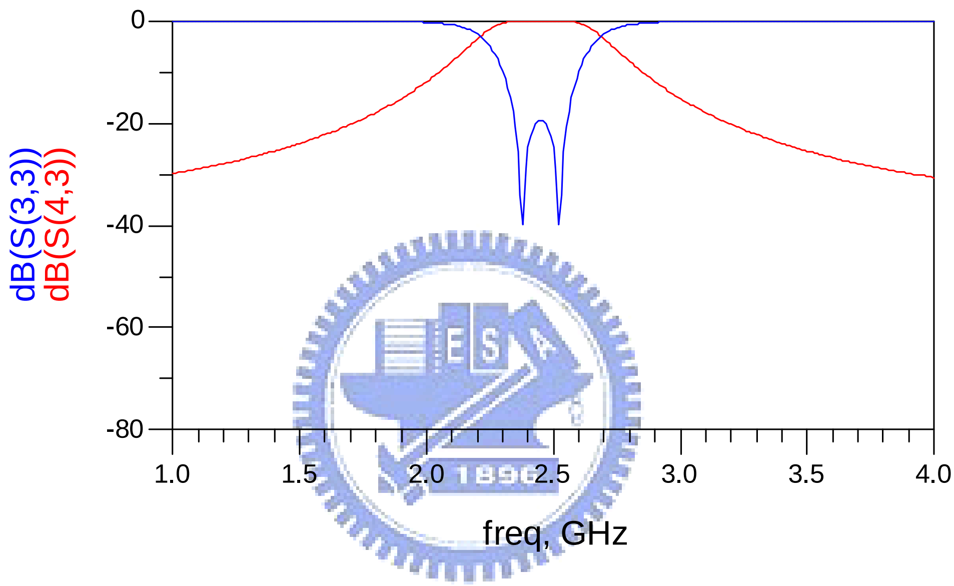

Figure 4.2: Narrow band ideal response of second order band-pass filter

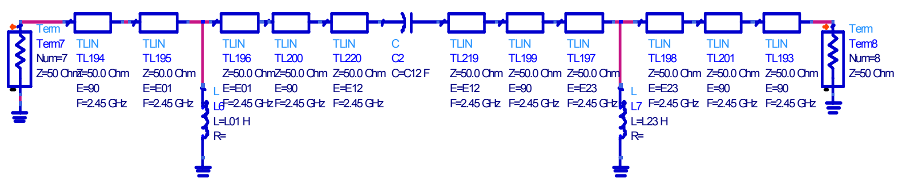

Figure 4.3: Equivalent circuit of second order band-pass filter

frequency f_0 is 2.45GHz, and fractional bandwidth Δ is 7 percent.

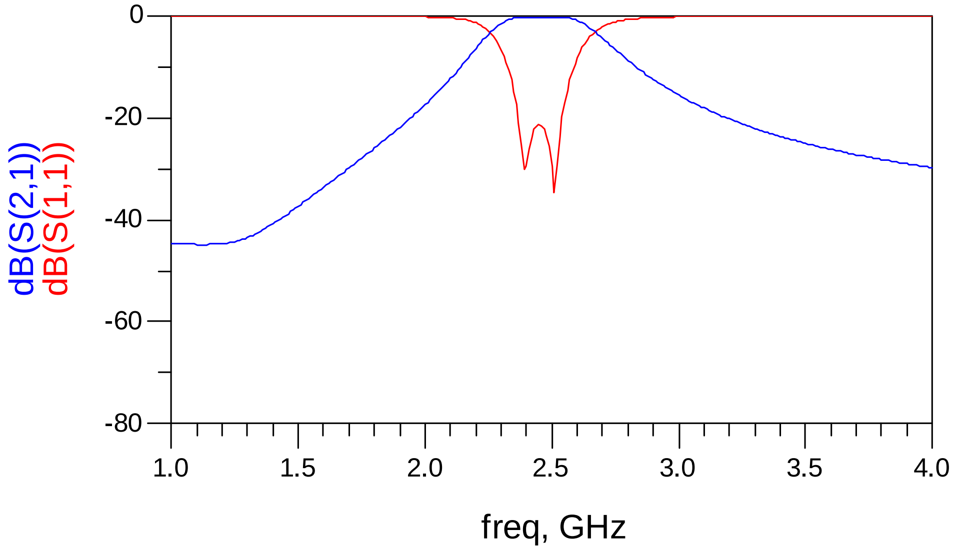

Figure 4.4: Narrow band differential mode simulation result

Circuit photo is shown in Fig. 4.5. The measured results are shown in Fig. 4.6 and 4.7. Fig. 4.5 shown center frequency f_0 is 2.4GHz, and fractional bandwidth Δ is 8 percent. Fig. 4.7 is shown broad band common mode response.

4.2 Third Order Band-Pass Filter

Repeat all steps as second order band-pass filter to design a third order filter. Its ideal circuit model is shown in Fig. 4.8, and its ideal circuit model simulated results are shown in Fig. 4.9. Fig. 4.9 shown center frequency f_0 is 2.45GHz, and fractional bandwidth Δ is 10 percent.

Following the same design steps as second order filter a initial physical design can

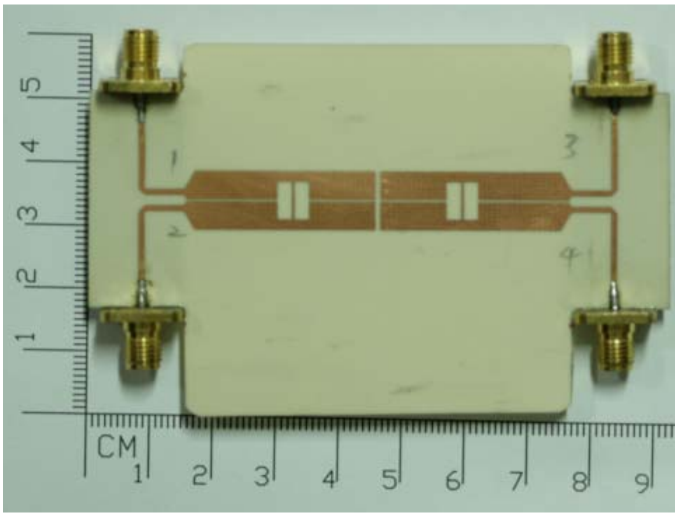

Figure 4.5: Photo of the second order band-pass filter

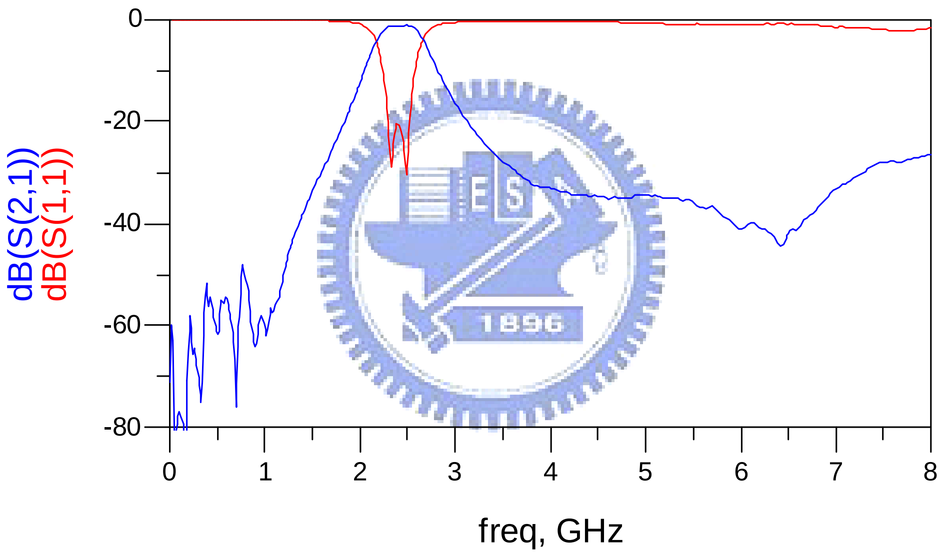

Figure 4.6: Broad band differential mode measurment result

be obtained in Fig. 4.10. After fine tuning, the EM simulated results are depicted in Fig. 4.11, which shown center frequency f_0 is 2.45GHz, and fractional bandwidth Δ is 8 percent.

Circuit photo is shown in Fig. 4.12. The measured results are shown in Fig. 4.13

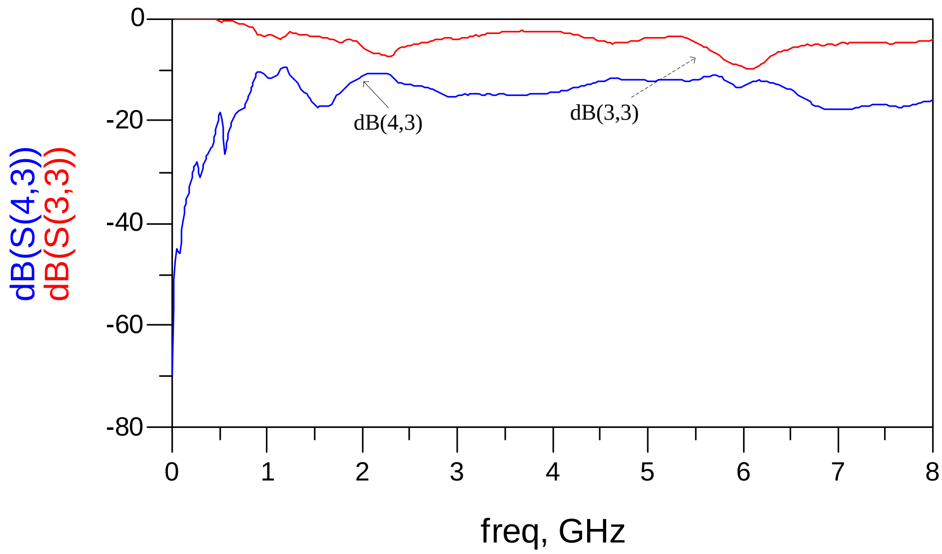

Figure 4.7: Broad band common mode measurment result

and 4.14. Fig. 4.13 shown center frequency f_0 is 2.42GHz, and fractional bandwidth Δ is 8 percent. Fig. 4.14 is shown broad band common mode response.

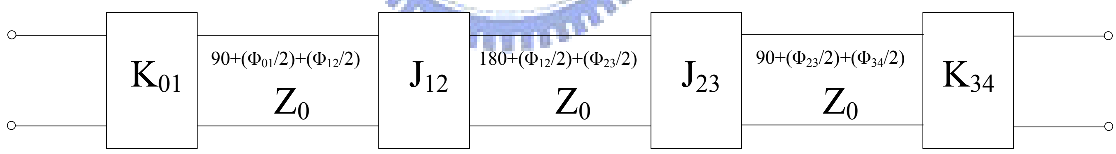

Figure 4.8: Half circuit model of a third order band-pass filter

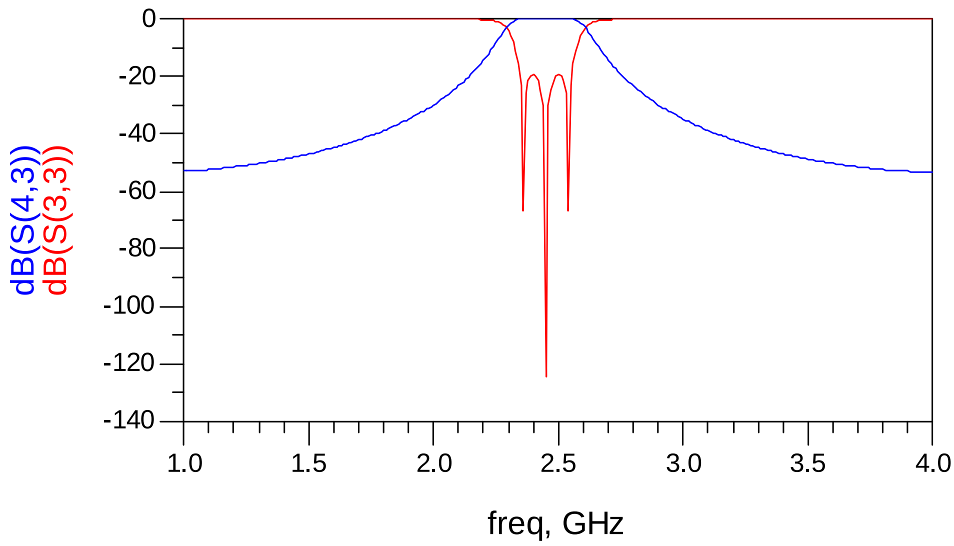

Figure 4.9: Narrow band ideal response of third order band-pass filter

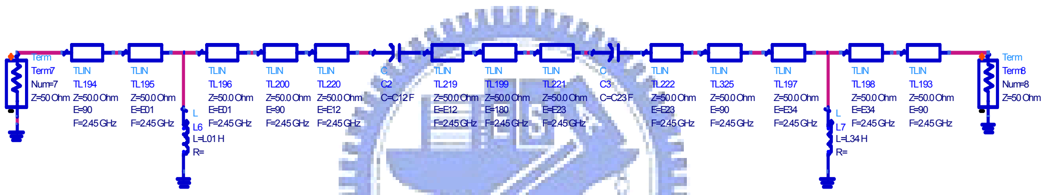

Figure 4.10: Equivalent circuit of third order band-pass filter

4.3 Fourth Order Band-Pass Filter

We try against to design fourth order band-pass filter for two kinds architecture.

4.3.1 Architecture-I

Its ideal model, ideal response, equivalent circuit, and EM-simulation are shown in Fig. 4.15-4.18, respectively.

Fig. 4.16 shown center frequency f_0 is 2.45GHz, and fractional bandwidth Δ is 15

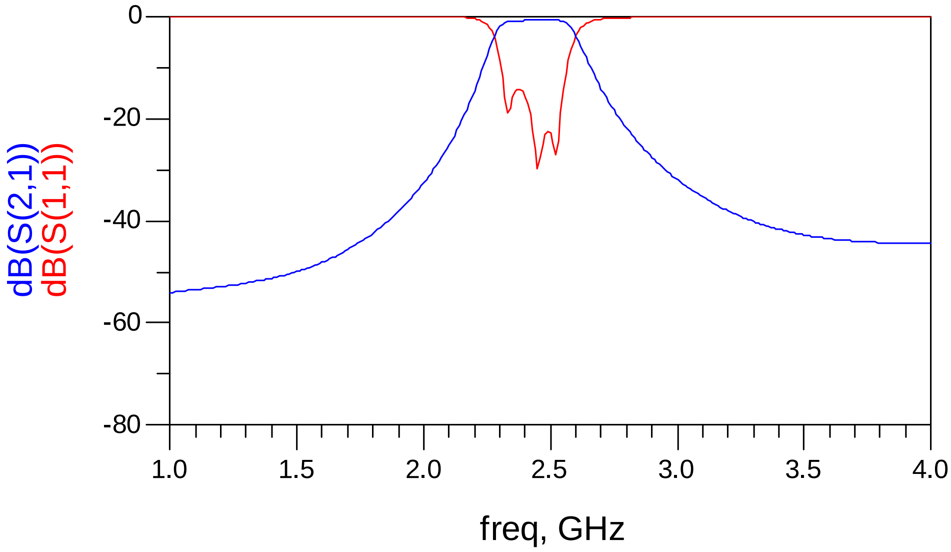

Figure 4.11: Narrow band differential mode simulation result

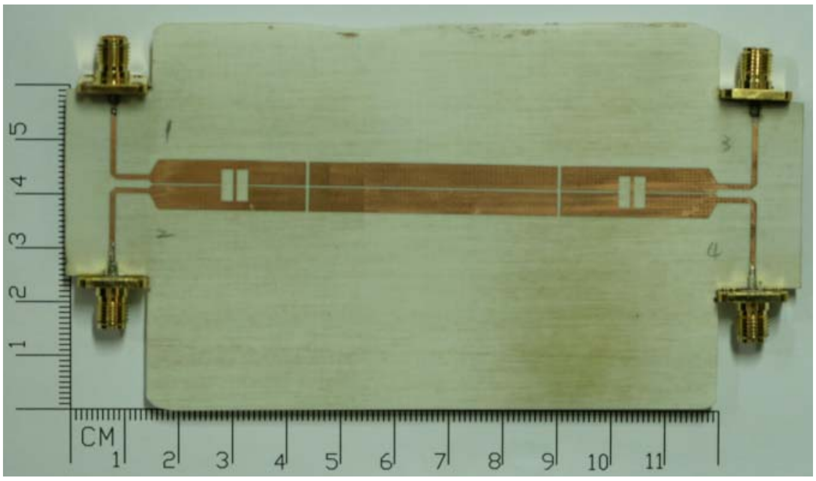

Figure 4.12: Photo of the third order band-pass filter

percent. Fig. 4.18 shown center frequency f_0 is 2.45GHz, and fractional bandwidth Δ is 15 percent.

Circuit photo is shown in Fig. 4.19. The measured results are shown in Fig. 4.20 and 4.21. Fig. 4.20 shown center frequency f_0 is 2.34GHz, and fractional bandwidth

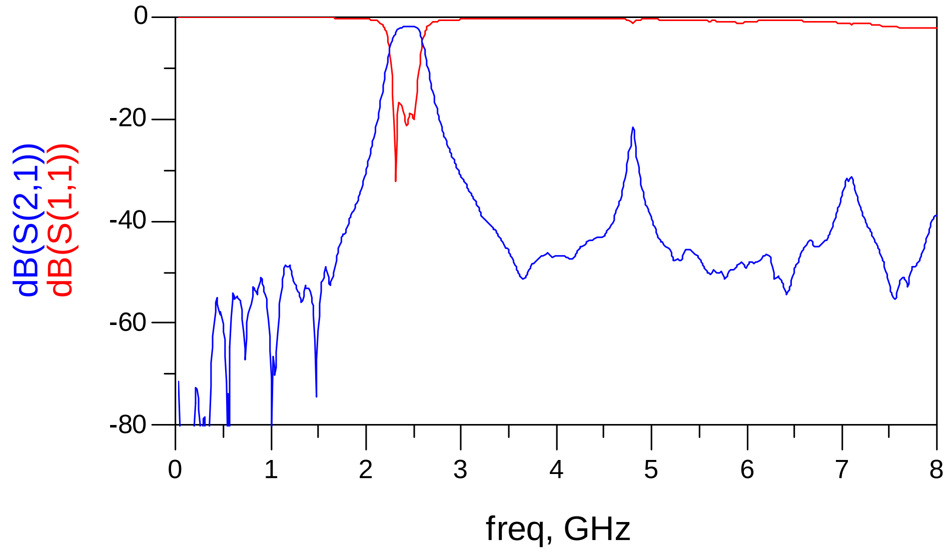

Figure 4.13: Broad band differential mode measurment result

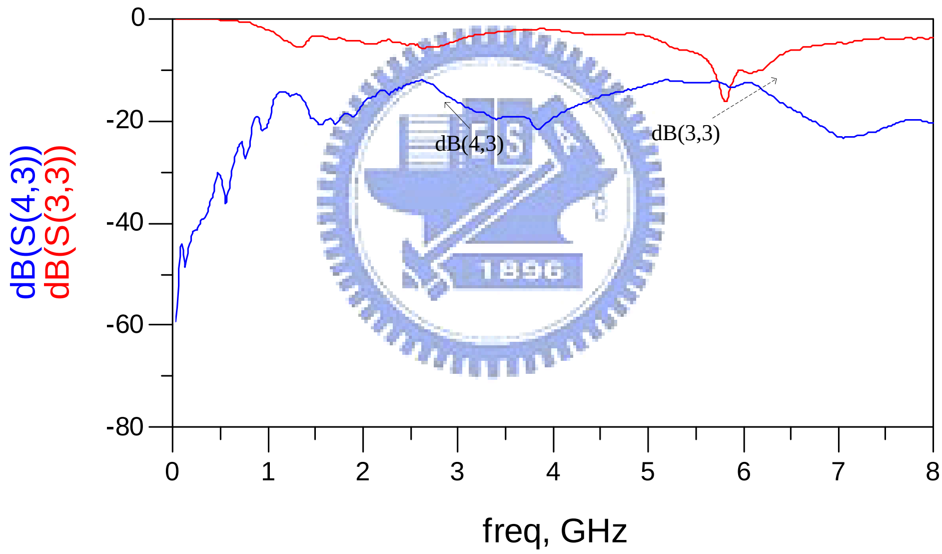

Figure 4.14: Broad band common mode measurment result

Δ is 15 percent. Fig. 4.21 is shown broad band common mode response.

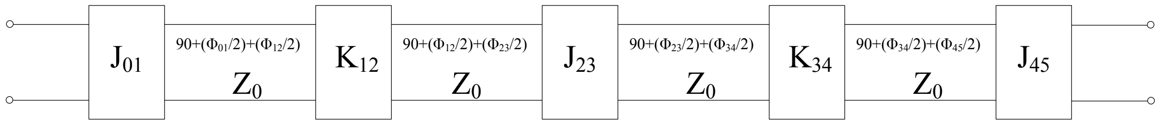

Figure 4.15: Half circuit model of a fourth order band-pass filter of architecture-I

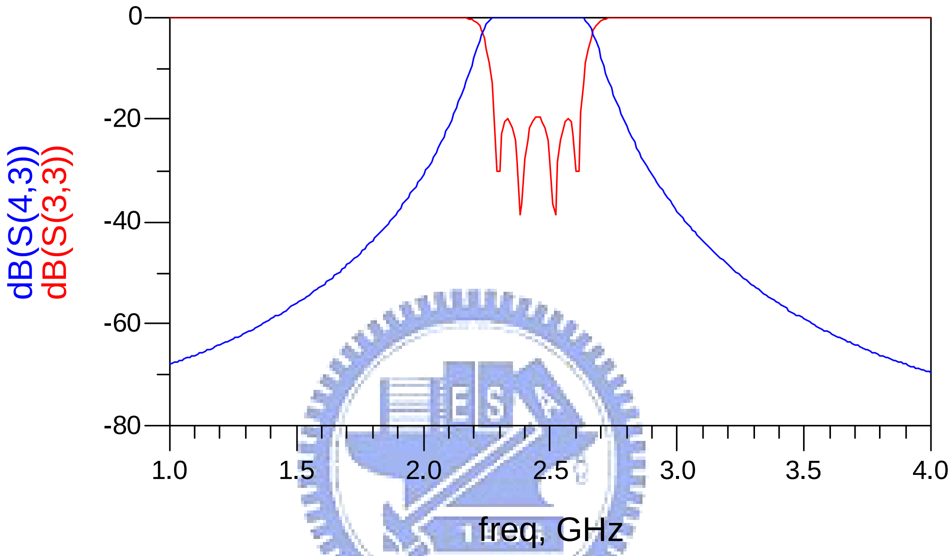

Figure 4.16: Narrow band ideal response of fourth order band-pass filter of architecture-I

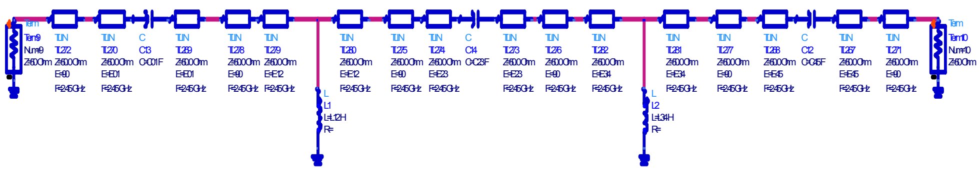

Figure 4.17: Equivalent circuit of fourth order band-pass filter of architecture-I

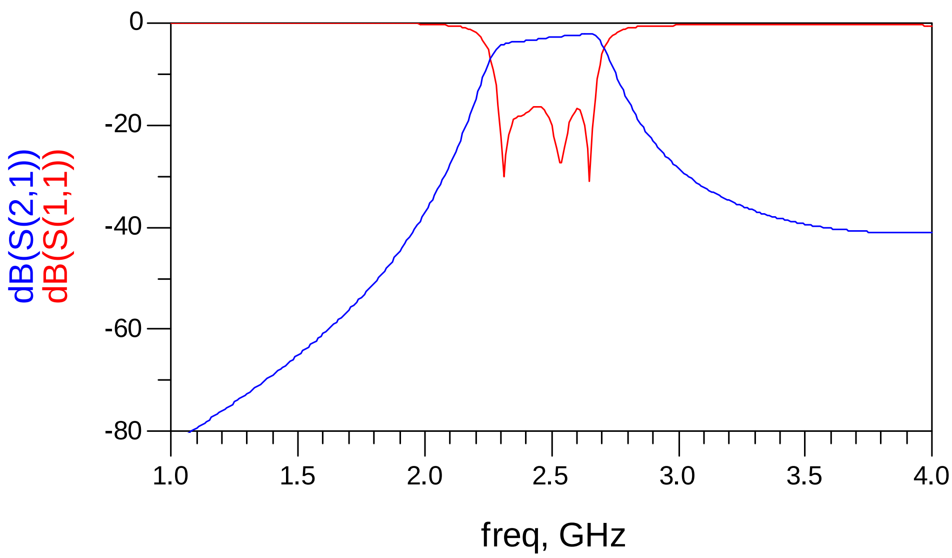

Figure 4.18: Narrow band differential mode simulation result of architecture-I

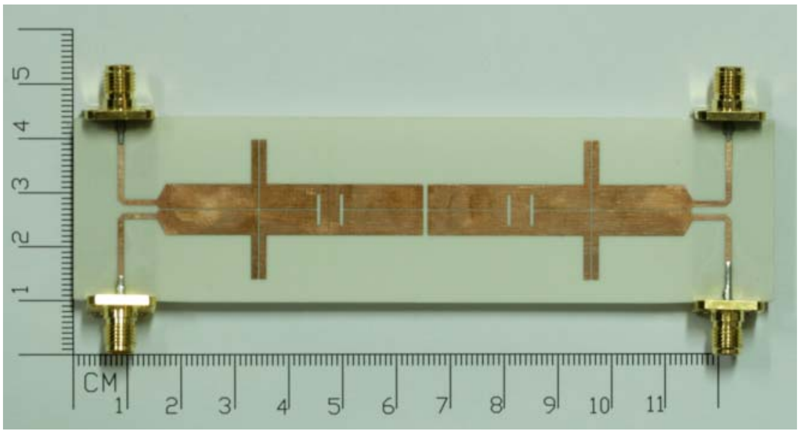

Figure 4.19: Photo of the fourth order band-pass filter I

4.3.2 Architecture-II

Its ideal model, ideal response, equivalent circuit, and EM-simulation are shown in Fig. 4.22-4.25, respectively. Circuit photo is shown in Fig. 4.26.

Fig. 4.23 shown center frequency f_0 is 2.45GHz, and fractional bandwidth Δ is 15 percent. Fig. 4.25 shown center frequency f_0 is 2.45GHz, and fractional bandwidth

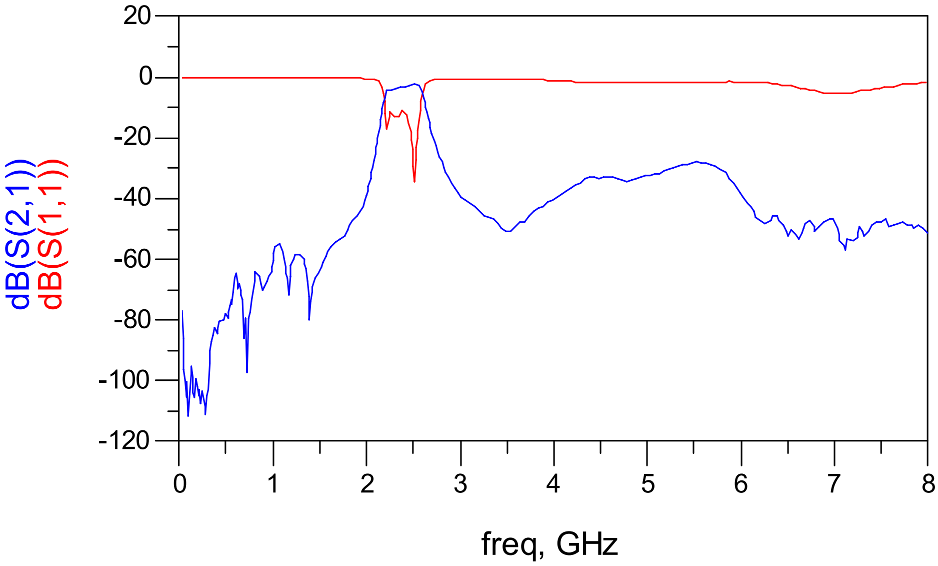

Figure 4.20: Broad band differential mode measurment result

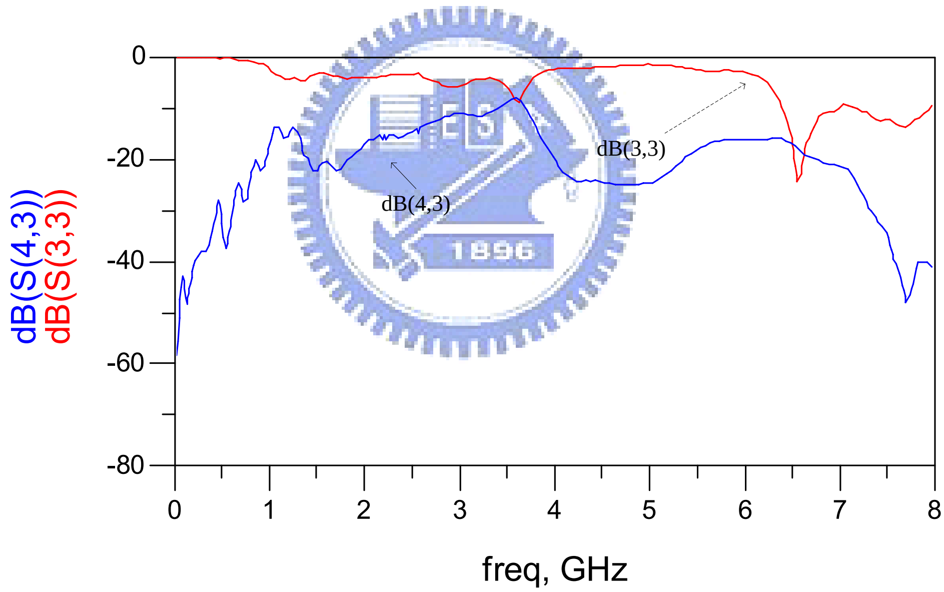

Figure 4.21: Broad band common mode measurment result

Δ is 14 percent.

The measured results are shown in Fig. 4.27 and 4.28. Fig. 4.27 shown center frequency f_0 is 2.34GHz, and fractional bandwidth Δ is 15 percent. Fig. 4.28 is shown broad band common mode response.

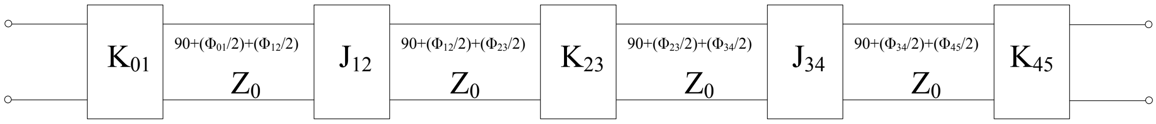

Figure 4.22: Half circuit model of a fourth order band-pass filter architecture-II

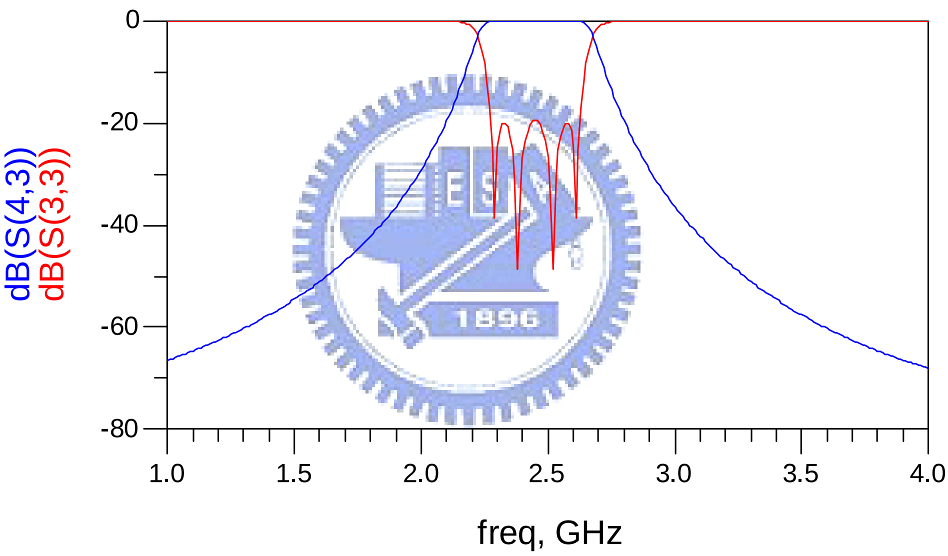

Figure 4.23: Narrow band ideal response of fourth order band-pass filter of architecture-II

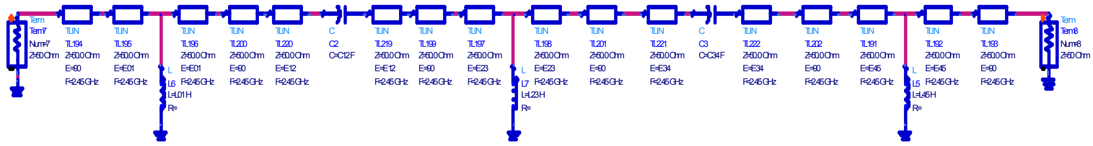

Figure 4.24: Equivalent circuit of fourth order band-pass filter of architecture-II

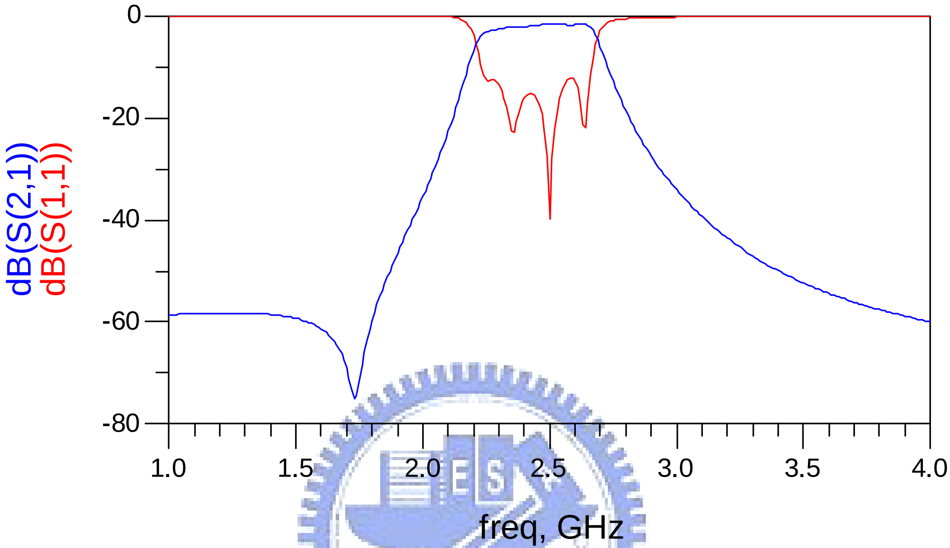

Figure 4.25: Narrow band differential mode simulation result of architecture-II

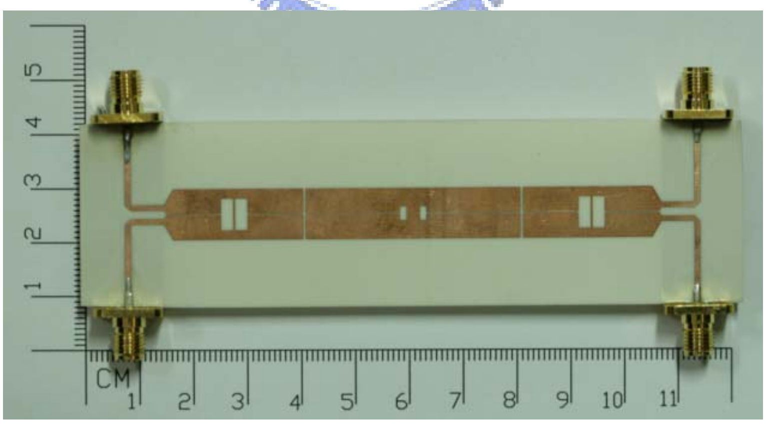

Figure 4.26: Photo of the fourth order band-pass filter II

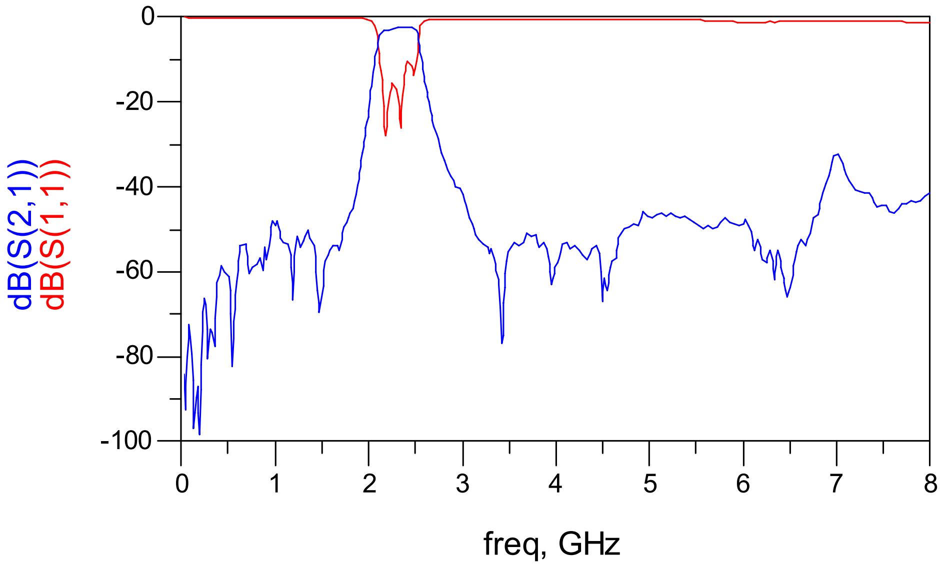

Figure 4.27: Broad band differential mode measurment result

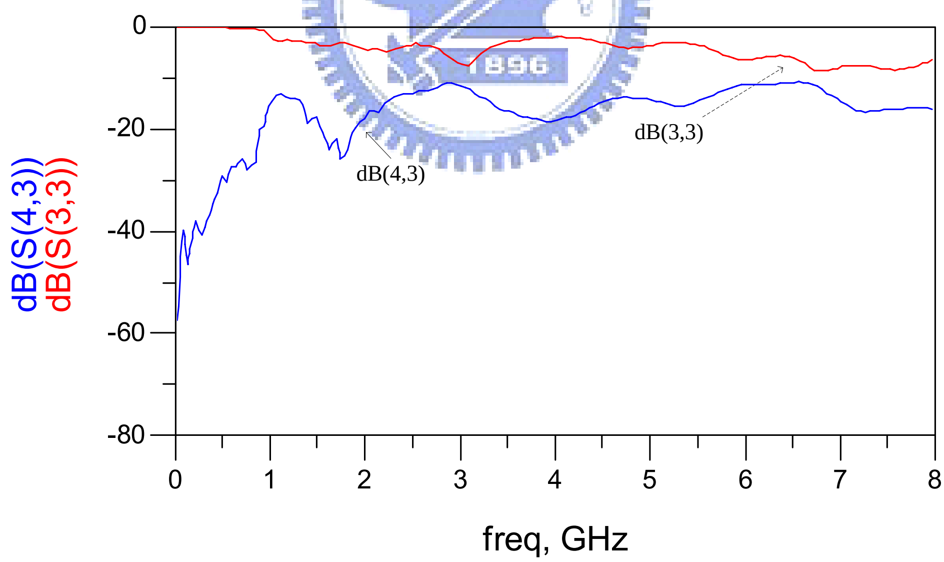

Figure 4.28: Broad band common mode measurment result

Chapter 5

Conclusion

In this thesis, we have proposed J and K inverters which are suitable for designing a CPS band-pass filters with $\lambda/2$ and $\lambda/4$ resonators. An analytical design procedure has been developed, the related design formulas have also been derived. The design curves to extract the series suceptance value and shunt reactance value for J and K inverters have also been achieved. Three types of transition circuits have been developed to extract the mixed-mode S-parameters of filters.

Several CPS bandpass filters have been designed and realized to demonstrate the feasibility of the proposed design method. The measured performances matched well to the simulated ones.

Bibliography

[1] *IEEE Standard 802.15.1*

[2] *IEEE Standard 802.15.4*

[3] *IEEE Standard 802.11.b/g*

[4] J. B. Knorr and K. D. Kuchler, "Analysis of coupled slots and coplanar striplines on dielectric substrate," *IEEE Trans. Microw. Theory Tech.*, vol. MTT-23, pp. 541-548, July. 1975.

[5] K. C. Gupta, R. Garg, I. Bahl, and P. Bhartia, Microstripline Lines and Slot Lines, Artech House, 1996.

[6] Rainee N. Simons, Coplanar Waveguide Circuits, Components, and Systems, John Wiley and Sons Inc., 2003.

[7] Kavita Goverdhanam, Rainee N. Simons, and Linda P. B. Katehi, "Coplanar stripline components forhigh-frequency applications," *IEEE Trans. Microw. Theory Tech.*, vol. 45, no. 10, pp. 1725-1729, Oct. 1997.

[8] Rainee N. Simons, Nihad I. Dib,and Linda P. B. Katehi, "Modeling of coplanar stripline discontinuities," *IEEE Trans. Microw. Theory Tech.*, vol. 44, no. 5, pp. 711-716, May. 1996.

[9] Lei Zhu, and Ke Wu, "Field-extracted lumped-element models of coplanar stripline circuits and discontinuities for accurate radio-frequency design and optimization," *IEEE Trans. Microw. Theory Tech.*, vol. 50, no. 4, pp. 1207-1215, Apr. 2002.

[10] Young-Ho Suh, and Kai Chang, "Coplanar stripline resonators modeling and applications to filters," *IEEE Trans. Microw. Theory Tech.*, vol. 50, no. 5, pp. 1289-1296, May. 2002.

[11] E. G. Cristal, and L. Young, "Field-extracted lumped-element models of coplanar stripline circuits and discontinuities for accurate radio-frequency design and optimization," *IEEE Trans. Microw. Theory Tech.*, vol. MTT-13, pp. 544-558, Sept. 1965.

[12] N. Yang and Z.N. Chen, "Serially-connected series-stub resonators for narrow-band coplanar stripline bandpass filters," *IEEEE Microw. Wireless Compon. Lett.*, vol 15, no. 12, pp. 835-837, Dec. 2005.

[13] Ning Yang, Christophe Caloz, Ke Wu,and Zhi Ning Chen, "Broadband and compact coupled coplanar stripline filters with impedance steps," *IEEE Trans. Microw. Theory Tech.*, vol.55, no. 12, pp. 2874-2886, Dec. 2007.

[14] Ning Yang, Christophe Caloz, Zhi ning Chen and Ke Wu, "Broadband and compact double stepped-impedance CPS filters with coupled-resonance enhanced selectivity," *IEEE MTT-S Int. Microw. Sym. Dig.* , in Honolulu, HI, Jun. 2007, pp. 755-758,

[15] Ning Yang, Christophe Caloz, and Ke Wu, "Co-designed CPS UWB filter-antenna System," *IEEE Int. Antennas Propag. Sym.* , pp. 1433-1436, Jun. 2007.

[16] J.-S. Hong and M.J Lancaster, Microstripline Filters for RF Microwave Applications, New York: Wiley, 2001.

[17] G.L Matthaei, L. Young, and E.M.T. Jones, Microwave Filters, Impedance-Matching Network, and Coupling Structures, Boston,MA: Artech House, 1964.

[18] D.M. Pozar, Microwave Engeineering,2nd ed., New York: Wiley, 1998.

[19] C.-H. Wu, C.-H. Wang, and C.H. Chen, "Balanced coupled-resonator bandpass filters using multisection resonators for common-mode suppression and stopband extension," *IEEEE Trans. Microw. Theory Tech.*, vol. 55, no. 8, pp. 1756-1763, Aug. 2007.

[20] Sergei A. Doberstein, and Vladimir K. Razgoniaev, "Balanced front-end hybrid SAW modules with impedance conversion," *IEEE Ultrasonics Sym.*, 2002.

[21] Chia-Cheng Chuang and Chin-Li Wang, "Design of three-pole single-to-balanced bandpass filters," ,in 36th Eur. Microw. Proc., Manchester, UK, Sep. 2006, pp.1193-1196.

[22] K. Entesai, T. V.-Heikkila and G..M. Rebeiz, "Miniaturized differential filters for C- and Ku-band applications," ,in 33rd Eur. Microw. Conf., Munich, Germany, Oct. 2003, pp. 227-229.

[23] W. Fan, Albert Lu, L.L. Wai, and B.K. Lok, "Mixed-mode S-parameter characterization of differential structures," *IEEE Electro. Packaging Tech. Conf.*, 2003, pp. 533-537.

[24] D.E. Bockelman and W.R. Eisenstadt, "Pure-mode network analyzer for on-wafer measurements of mixed-mode S-parameters of differential circuits," *IEEE Trans. Microw. Theory Tech.*, vol. 45, no. 7, pp. 1071-1077, July. 1997.

[25] D.E. Bockelman and W.R. Eisenstadt, "Combined differential and common-mode scattering parameters theory and simulation," *IEEE Trans. Microw. Theory Tech.*, vol. 43, no. 7, pp. 1530-1539, July. 1995.